

**MICROWAVE SYNTHESIS OF
ZnO/rGO NANOCOMPOSITES FOR
ENHANCED DEGRADATION OF DYE**

FATIN SAIHA BINTI OMAR

**FACULTY OF SCIENCE
UNIVERSITY OF MALAYA
KUALA LUMPUR**

2014

UNIVERSITI MALAYA
ORIGINAL LITERARY WORK DECLARATION

Name of Candidate: **Fatin Saiha binti Omar**

(I.C/Passport No: **880324-56-5090**)

Registration/Matric No: **SGR110111**

Name of Degree: **Master of Science (Dissertation)**

Title of Dissertation ("this Work"):

**MICROWAVE SYNTHESIS OF ZnO/rGO NANOCOMPOSITES FOR ENHANCED
DEGRADATION OF DYE**

Field of Study: Low Dimensional Materials

I do solemnly and sincerely declare that:

- (1) I am the sole author/writer of this work;
- (2) This work is original;
- (3) Any use of any work in which copyright exists was done by way of fair dealing and for permitted purposes and any excerpt or extract from, or reference to or reproduction of any copyright work has been disclosed expressly and sufficiently and the title of the Work and its authorship have been acknowledged in this Work;
- (4) I do not have any actual knowledge nor do I ought reasonably to know that the making of this work constitutes an infringement of any copyright work;
- (5) I hereby assign all and every rights in the copyright to this Work to the University of Malaya ("UM"), who henceforth shall be owner of the copyright in this Work and that any reproduction or use in any form or by any means whatsoever is prohibited without the written consent of UM having been first had and obtained;
- (6) I am fully aware that if in the course of making this Work I have infringed any copyright whether intentionally or otherwise, I may be subject to legal action or any other action as may be determined by UM.

Candidate's Signature

Date:

Subscribed and solemnly declared before,

Witness's Signature

Name: **Dr. Huang Nay Ming**

Date:

ABSTRACT

Zinc oxide/reduced graphene oxide (ZnO/rGO) nanocomposites were successfully synthesized in the presence of diethylenetriamine (DETA) via a facile microwave assisted method. The x-ray diffraction (XRD) patterns of the ZnO/rGO nanocomposites reveal that obtained nanocomposite materials containing ZnO in hexagonal phase with wurtzite structure. The high-resolution transmission electron microscopy (HRTEM) images indicates that the prepared nanocomposites having ZnO nanorods, with an average length:diameter ratio of 10 and which is found to be deposited onto the rGO sheets. Under the irradiation of sunlight, the ZnO/rGO nanocomposites showed two-fold improved photocatalytic performance than that of unmodified ZnO towards the photodegradation of methylene blue. This may due to the high adsorbitivity of ZnO/rGO nanocomposite and synergistic effect raised between smaller ZnO nanorods and rGO matrix led to the improved photocatalytic activity. Further, the ZnO/rGO nanocomposites showed six-fold enhanced photocurrent response than that of bare ZnO nanorods. The excellent photocatalytic performance of the newly prepared ZnO/rGO nanocomposites could be a potential candidate for the photocatalysis and photoelectrochemical applications.

ABSTRAK

Zink oksida/dikurangkan graphene oksida (ZnO/rGO) nanokomposit telah berjaya disintesis dengan kehadiran diethylenetriamine (DETA) melalui kaedah mudah gelombang mikro. Corak pembelauan sinar-x (XRD) nanokomposit ZnO/rGO mendedahkan bahawa bahan-bahan nanokomposit yang didapati mempunyai ZnO dalam fasa heksagon dengan struktur wurtzite. Imej resolusi tinggi elektron penghantaran mikroskop (HRTEM) menunjukkan bahawa nanokomposit mempunyai nanorod ZnO, dengan purata nisbah panjang:diameter 10 dan didapati didepositkan pada helaian rGO. Di bawah penyinaran cahaya matahari, nanokomposit ZnO/rGO menunjukkan dua kali ganda prestasi baik fotokatalitik daripada tidak ubahsuai ZnO ke arah fotodegradasi metilena biru. Ini mungkin disebabkan penyerapan yang tinggi oleh nanokomposit ZnO/rGO dan kesan sinergistik dibangkitkan antara nanorod ZnO yang lebih kecil dan rGO matriks yang membawa kepada aktiviti fotokatalisis yang bertambah baik. Lagi nanokomposit ZnO/rGO menunjukkan peningkatan enam kali ganda arusfoto balas daripada nanorod ZnO. Prestasi fotokatalitik yang sangat baik oleh penyediaan baru nanokomposit ZnO/rGO boleh menjadi calon yang berpotensi untuk aplikasi fotokatalisis dan fotoelektrokemikal.

ACKNOWLEDGMENT

First and foremost, I would like to thank God “the almighty Allah”, whose many blessings have made me who I am today. I am deeply and forever indebted to my parents and all my siblings for their love and support they have given me throughout my entire life. There are several people with whom I am indebted for their help and contributions in this course of research work.

I am truly thankful to my supervisor, Dr. Huang Nay Ming, who not only gave me opportunity to conduct research under his supervision, but also showed me his tremendous help, support, patience and guidance in all stages of this thesis. I am thankful for being part of the group under his supervision as he has always been concerned with the development of us. My special thanks also go to Dr. Janet Lim Hong Ngee for her relentless efforts in guiding me throughout this research work. And also never forget to Dr. Vijay Kumar and Dr. Pandikumar Alagarsamy, for being a reliable person to whom I could always talk about my problems and encouraging me to shape my interest in this research work. It would have been impossible to write this thesis without their help and valuable advices.

In the completion of this work, my sincere thanks go to all the people in the Low Dimensional Materials Research Center (LDMRC) lab, who made the lab a friendly environment for working. I would like to acknowledge Mr Mohamad and Mrs Lorlela for the technical assistance, and more thanks to all my colleagues for their knowledgeable, support, and help especially to Peik See, Gregory, Syed, Supei, Mazlinda, Marlinda, Rina, An’amt, Betty, Saipul, Azrina and Linda.

Last but not least, I would like to thank University of Malaya (UM) for providing me the High Impact Research Grant (UM.C/625/1/HIR/030) and Postgraduate Research Fund (PG107-2012B), the Ministry of Higher Education for High Impact Research Grant

(UM.C/625/1/HIR/MOHE/05) and Loreal Malaysia “For Women in Science Fellowships”
2011 (6375900-10501).

LIST OF PUBLICATION

1. **Fatin, S. O.**, Lim, H. N., Tan, W. T., **Huang, N. M***. (2012). Comparison of Photocatalytic Activity and Cyclic Voltammetry of Zinc Oxide and Titanium Dioxide Nanoparticles toward Degradation of Methylene Blue. **International Journal of Electrochemical Science**, 7, 9074-9084.
2. **Fatin, S. O.**, **Huang N. M.***, Syed M. H., Lim H. N. (2014). Microwave Synthesis of Zinc Oxide/Reduced Graphene Oxide Hybrid for Adsorption-Photocatalysis Application. **International Journal of Photoenergy**. 2014, Article ID 176835 (8 pages)

TABLE OF CONTENT

ABSTRACT	iii
ABSTRAK	iv
ACKNOWLEDGMENT	v
LIST OF PUBLICATION	vii
LIST OF FIGURES	x
LIST OF TABLES	xii
LIST OF ABBREVIATIONS	xiii
CHAPTER 1 : INTRODUCTION.....	1
1.1 Research background.....	1
1.1.1 Nanoscience and Nanotechnology	1
1.1.2 Semiconductor nanoparticle	2
1.1.3 Background of reduced graphene oxide and zinc oxide	2
1.2 Research problems and motivations	4
1.3 Research objectives	5
1.4 Thesis outline.....	5
CHAPTER 2 : LITERATURE REVIEW.....	8
2.1 Introduction	8
2.2 Microwave.....	8
2.2.1 Principle.....	9
2.3 Zinc oxide (ZnO).....	11
2.3.1 Synthesis and growth mechanisms in alkaline solutions	13
2.4 Titanium dioxide (TiO ₂).....	14
2.4.1 Comparison between ZnO and TiO ₂ in photocatalysis.....	14
2.5 Graphene	15
2.6 Graphite oxide/graphene oxide (GO)	16
2.7 Reduced graphene oxide (rGO)	17
2.8 Zinc oxide/reduced graphene oxide (ZnO/rGO) nanocomposites	18
2.9 Diethylenetriamine	20
2.10 Heterogeneous photocatalysis.....	21
2.10.1 Methylene blue	22
2.10.2 Photocatalytic properties of ZnO/rGO nanocomposite	23
2.11 Photoelectrochemical processes.....	26
2.12 Photoelectrochemical measurement	26
2.13 Cyclic Voltammetry (CV).....	28

2.14	Photocurrent	30
CHAPTER 3 : EXPERIMENTAL METHODS		32
3.1	Introduction	32
3.2	Part I	32
3.2.1	Materials	32
3.2.2	Experimental	32
3.2.3	Application methods	33
3.3	Part II	35
3.3.1	Material.....	35
3.3.2	Experimental	35
3.3.3	Application methods	38
3.4	Characterization techniques.....	40
3.4.1	X-Ray Diffraction (XRD)	40
3.4.2	Ultraviolet-Visible (UV-Vis) Spectroscopy.....	41
3.4.3	Raman spectroscopy.....	42
3.4.4	Field Emission Scanning Electron Microscopy (FESEM)	42
3.4.5	High Resolution Transmission Electron Microscope (HRTEM).....	43
3.4.6	X-ray Photoelectron Spectroscopy (XPS)	43
CHAPTER 4 : RESULTS AND DISCUSSION		45
4.1	Introduction	45
4.2	Part I	46
4.2.1	Characterizations of nanomaterials	46
4.2.2	Applications	49
4.3	Part II	56
4.3.1	Characterization of nanocomposites	56
4.3.2	Applications	66
CHAPTER 5 : CONCLUSION AND FUTURE WORKS		70
5.1	Conclusion.....	70
5.2	Future works	72
REFERENCES		73

LIST OF FIGURES

Figure 2.1 Dipolar rotation (Tierney & Westman, 2001).....	9
Figure 2.2 Ionic conduction (Tierney & Westman, 2001)	10
Figure 2.3 ZnO crystal structures; (a) cubic rock salt (b) cubic zinc blende, and (c)hexagonal wurtzite (Hadis Morkoç & Ümit Özgür, 2009).....	12
Figure 2.4 Growth habits of ZnO nanoparticles (Bai et al., 2011)	14
Figure 2.5 Crystal structure of (a) rutile (b) anatase (c) brookite (Freitas et al., 2013)	14
Figure 2.6 Graphene structure (Hedberg, 2013).....	15
Figure 2.7 Unit cell of graphene (Hatsugai, 2010).....	16
Figure 2.8 Formation of σ bond and π orbital in graphene (Srivastava, 2012).....	16
Figure 2.9 Chemical structure of graphene oxide (Park & Ruoff, 2009)	17
Figure 2.10 Schematic mechanism of oxidation of graphite producing GO and chemical reduction of GO producing rGO (Kauppila & Viinikanoja, 2012)	18
Figure 2.11 A proposed schematic route for decorating ZnO onto rGO sheets. (1) Interaction of Zn ion with the oxygenated group of GO. (2) Formation of ZnO/rGO composite.....	20
Figure 2.12 Chemical structure of Diethylenetriamine	20
Figure 2.13 Chemical structure of methylene blue (Adams et al., 2007).....	22
Figure 2.14 Methylene blue solution.....	22
Figure 2.15 Two proposed mechanisms of photocatalytic activity of MB by ZnO/rGO composite (Adán-Más & Wei, 2013)	25
Figure 2.16 Schematic diagram of a conventional three-electrode cell	28
Figure 2.17 Cyclic voltammetry voltage sweep (Gouws, 2012).....	29
Figure 2.18 Typical cyclic voltammogram	30
Figure 2.19 Typical photocurrent graph.....	31
Figure 3.1 (a) Preparation of immobilized photocatalyst before calcination	33
Figure 3.2 Photoelectrochemical setup.....	34
Figure 3.3 The reaction process of Simplified Hummers method (a) before 3 days oxidation (b) after 3 days oxidation.....	36
Figure 3.4 Graphene oxide gel	36
Figure 3.5 Microwave (model: NN-S553WF)	37
Figure 3.6 (a) GO (b) rGO (c) ZnO in the presence of DETA (d) ZnO in the absence of DETA	37
Figure 3.7 Working electrode; (a) ZnO (b) ZnO/rGO nanocomposite coated on ITO glass ..	39
Figure 3.8 Screenshot of PANalytical X'pert Highscore software.....	40
Figure 3.9 Thermo Fisher Scientific Evolution 300 UV-Vis spectrometer.....	41
Figure 3.10 Renishaw inVia Raman microscope	42
Figure 3.11 Screenshot of Visual Basic Macro software	44
Figure 4.1 XRD patterns of (ai) calcined ZnO powder, (aii) calcined ZnO film, (aiii) ZnO pure powder (bi) calcined P25 powder, (bii) calcined P25 film, (biii) P25 pure powder	46
Figure 4.2 UV-Vis spectra of ZnO and P25	47
Figure 4.3 SEM images of (a) calcined ZnO powder, (b) calcined immobilized ZnO, (c) calcined P25 powder and (d) calcined immobilized P25	48
Figure 4.4 UV-Vis absorption spectra of the MB solution (a) without photocatalyst, (b) with photocatalyst under UV light, and (c) with photocatalyst under solar light illumination	49

Figure 4.5 a) CV and (b) multiple CV of modified GCE in 0.1 M of KCl solution with and without the presence of 1.5 ppm of MB	51
Figure 4.6 CV for (a) bare GCE, (b) ZnO-modified GCE, and (c) P25-modified GCE in 0.1 M of KCl solution spiked with 1.5 ppm of MB left in the dark for 2 hours	53
Figure 4.7 CV for (a) bare GCE, (b) ZnO-modified GCE, and (c) P25-modified GCE in 0.1 M of KCl solution spiked with 1.5 ppm of MB illuminated with solar light for 2 hours (m: minutes)	54
Figure 4.8 Immobilized P25 and ZnO film after the photocatalysis process	55
Figure 4.9 XRD patterns of GO, rGO, ZnO, ZG1, ZG2 and ZG3	56
Figure 4.10 UV-Vis spectra of GO, rGO, ZnO, ZG1, ZG2 and ZG3	58
Figure 4.11 Raman spectra of GO, rGO, ZnO, ZG1, ZG2 and ZG3	59
Figure 4.12 XPS spectra of (a) C1s of GO and ZG1, (b) O1s of ZnO and ZG1	61
Figure 4.13 FESEM images of (a) ZnO, (b) ZG1 and (c) ZG	63
Figure 4.14 EDX spectrum of ZG1 nanocomposite	64
Figure 4.15 HRTEM images of (a) ZnO, (b) ZG3, (c) ZG2, (d) ZG1 and (e) ZG1 at a higher magnification	65
Figure 4.16 (a) Adsorption performance of ZnO, ZG1, ZG2 and ZG3 in the dark. (b) Photodegradation performance of blank (without photocatalyst), ZnO, ZG, ZG1, ZG2 and ZG3 under the sunlight	66
Figure 4.17 Cycling runs in the photodegradation of MB by ZG1 under the sunlight	67
Figure 4.18 HRTEM image of (a) ZG1 before photocatalysis (b) ZG1 after six cycles	67
Figure 4.19 Photocurrent of ZnO, ZG, ZG1, ZG2 and ZG3 under solar light irradiation	68

LIST OF TABLES

Table 1 Differences between microwave and conventional heating technique (Kappe et al., 2009).....	11
Table 2 Function of electrochemical components (Gamry Instruments, 2013)	26

LIST OF ABBREVIATIONS

ZnO/rGO	Zinc oxide-reduced graphene oxide nanocomposites
ZnO	Zinc oxide
TiO ₂	Titanium dioxide
GO	Graphene oxide
rGO	Reduced graphene oxide
DETA	Diethylenetriamine
XPS	X-ray Photoelectron Spectroscopy
XRD	X-Ray Diffraction
UV-vis	Ultraviolet-Visible
FESEM	Field Emission Scanning Electron Microscopy
HRTEM	High Resolution Transmission Electron Microscopy
GCE	Glassy carbon electrode
ITO	Indium-tin oxide
WE	Working electrode
Ag/AgCl	Silver-silver chloride
CV	Cyclic voltammetry
i _p	Peak current

CHAPTER 1 : INTRODUCTION

1.1 Research background

1.1.1 Nanoscience and Nanotechnology

Nanoscience is a branch of science that mainly deals about the fundamental principles of molecules and structures having at least one dimension with size range of 1 and 100 nm. Nanotechnology is an emerging technology that mainly focuses about the synthesis, processing and applications of materials in nanoscale. The following nanoscale dimensions provide an idea to understand this size range: $1\text{ nm} = 10\text{ \AA} = 10^{-9}\text{ m}$ and $1\text{ }\mu\text{m}$ (*i.e.*, 1 micron) $= 10^{-4}\text{ cm} = 1000\text{ nm}$. For example, oxide materials having a diameter of one oxygen ion is about 1.4 \AA . Hence, seven oxygen ions will combine to bring a size of around 10 \AA or 1 nm , *i.e.*, the ‘lower’ side of the nano range. Nanoscale materials have been discovered and met tremendous interest by scientific research in generating innovations in many fields. Many great contributions have been created in the last few years such as medicine, electronics, advanced material, environmental technology etc. Nanomaterial is made up from at least a cluster of molecules. They are often looked as a key for a sustainable future due to their extremely small feature sized typically between 1-100 nm along at least one dimension, which is the intermediate size between isolated atoms and bulk macroscopic materials. The smallness of the particle relative to the bulk atoms causes some changes in the particle properties such as catalytic and chemical reactivity, electrical resistivity, and adhesion. With decreasing in size, it represents an increase collective active surface area, thus results in higher chemical reactivity. The fact, physical and chemical properties of the material depend on the surface properties as surfaces control the flow of a material or energy across an interface of material and its surrounding (Hickman, 2002).

1.1.2 Semiconductor nanoparticle

Semiconductor is most commonly employed nanomaterials in multifunctional applications including photocatalysis, photoelectrochemical cells, dye-sensitized solar cells and sensor devices. Literally, “semi” means partial while “conductor” means material that able to conduct electricity. A semiconductor is a material that can conduct electricity not as good as conductor/metal, but better than insulator. The conductivity and reaction efficiency of semiconductor can be altered or enhanced by adding some amounts of impurities (doping) or by interaction with external force such as light or temperature, or electric field. With these properties, semiconductor is often chosen as the material for constructing a device or catalyst.

Semiconductor nanomaterials consist of valence band (VB), where charge carriers (e.g. electrons and holes) are located, and conduction band (CB), where no charge carriers exist. It can be classified into two types; intrinsic which is chemically pure and has poor conductivity, and extrinsic which is improved intrinsic semiconductor. Intrinsic semiconductor has equal number of electron and hole. While for extrinsic semiconductor, the conductivity is improved by doping process which can produces two groups; n-type and p-type. The advantage of using semiconductor is it provides band gap that offers the mobility of electron-hole pairs. The activation of semiconductor photocatalyst depends on the electron-hole pairs created in the presence of light. Usually, semiconductor photocatalyst is commonly used in purifying and nature’s cleaning as it has photobleaching properties (Nandita & Amitava, 2004)

1.1.3 Background of reduced graphene oxide and zinc oxide

Graphene is a two-dimensional of a single layer carbon atom which is said to be the strongest and the most conductive of any material. It was first discovered by Phillip Wallace and was further studied by Andre Geim and Konstantin Novoselov from University of Manchester. In 2010, for this invention, they are awarded the Nobel Prize in Physics for their

“groundbreaking experiments regarding the two-dimensional material graphene” (Johnston, 2010).

Due to its amazing properties, it is needed for large scale applications such as wastewater treatment, solar cells, supercapacitor, batteries etc. The major limitation is production of graphene into the large scale with low cost is the challenge being faced till date. In the past, besides Tang Lau method and other methods, such as chemical vapor deposition (CVD) and exposure to strong pulse light, chemical reduction of GO is one usually chosen as an effective and low cost method to obtain massive yield of graphene-like materials or reduced graphene oxide (rGO). The rGO has almost similar properties as pristine graphene although it displays lower theoretical potential mainly in terms of conductivity and surface area. However, this does not mean that the rGO is effectively unusable. Through chemical reduction, the oxygen and defects level could be reduced and graphene domains will be increased thus could regain the conductivity of rGO (Tang et al., 2012).

Zinc oxide (ZnO) is the oxidized zinc metal which is one of the widely studied semiconductor in the metal oxide family besides TiO_2 . It is cheap and abundant material that has been used in various applications such as transparent conductive oxide, solar cells and sensors. ZnO is nontoxic nature, possess high photochemical reactivity and could absorb a large fraction of solar spectrum which makes it a promising candidate and alternative to TiO_2 to be applied in environmental photocatalysis (Ong, 2013).

Direct discharge of effluents such as pigments and dyes by textile industries to nearby rivers endangers the aquatic lives. Some of the materials like heavy metals complex used in the making of pigments and dyes are highly toxic. Besides the toxicity of the material, the color would blocks the sunlight from transmit through the water, causing reduction of photosynthetic action and disturbance to the natural growth cycles of the living organisms in the water. Conventional biological treatments are not really efficient to remove the dye contaminated

water. Photocatalysis is generally proposed for this type of water pollution treatment by mineralizing the organic compounds in wastewater into the simplest compounds. The study on this process started in 1972, where Fujishima and Honda discovered the photochemical water splitting by TiO_2 photocatalyst. Since then, semiconductor/rGO nanocomposite photocatalysts have been studied extensively because of combination properties of carbon as an absorber and provides electron mobility, and semiconductor as a photocatalyst. Therefore, nanocomposite is expected could efficiently overcome this environmental problem in a cost effective manner (Umar & Aziz, 2013).

1.2 Research problems and motivations

In photocatalysis, the photodegradation of pigment and dye by ZnO photocatalyst is still considered inefficient under solar light due to its wide band gap that requires higher energy light irradiation and rapid recombination of generated electron-hole pairs. In addition, the photocatalytic activity of ZnO has been found to be related to the properties of ZnO produced. The presence of defects and preparation method might influence the photocatalytic performance. Thus, it is essential to modify the ZnO photocatalyst production so that the photocatalytic performance could be enhanced and stable for a longer running time.

ZnO possess high surface energy which has a tendency to agglomerate. Agglomeration affects the active surface area (where the reactions occur) of the particles. The active surface area decreases when the size of particles larger, thus would lower the surface reactivity. If the density of the particles larger than the density of the solvent, the particles eventually sink under gravity to the bottom. This phenomenon would affect the performance of the catalyst in photocatalysis application.

There are various ways to minimize their high surface energy and one of the methods is composites. The insertion of ZnO particles into rGO could help in exfoliating GO which theoretically could prevent the stacking of graphene sheets and at the same time could decrease

the particle size. However, composite without any organic additive could not promise the stability of the synthesized particles. The size might still larger, the graphene sheets might be stacking back or even the morphology will not be uniform. Thus, organic additive need to be added as one alternative for synthesizing stable ZnO/rGO nanocomposite. Diethylenetriamine (DETA) acts as capping agent which can stabilize the deposition of ZnO particle into the rGO and also can control the morphology of the sample.

1.3 Research objectives

The objectives of this project are;

- 1) To investigate the photocatalytic performance of commercial powder ZnO and TiO₂ (P25) for the photodegradation by choosing methylene blue solution as model pollutant.
- 2) To synthesize nanocomposites with favorable properties by establishing the optimum parameters such as stirring time, GO loading, and amount of DETA. GO will be prepared using simplified Hummer's method and the sample will be synthesized using household microwave.
- 3) To analyze the synthesized samples in terms of structure and morphological properties, and the effect of defects present in ZnO.
- 4) To study the photocatalytic efficiency of the synthesized samples in photodegradation of methylene blue solution. The stability of the samples will be tested by repeating the photocatalysis experiment. The sample also will be run through photocurrent analysis to correlate with photocatalysis experiment.

1.4 Thesis outline

This thesis consists of five chapters and for overall, it has two parts. Part I deals about the comparative studies on the photocatalytic performance of commercial ZnO and P25, and

Part II discuss about the synthesis, characterization and photocatalytic activity of ZnO and ZnO/rGO nanocomposites. Below is a brief outline of the chapters:

Chapter 2: Literature review

This chapter begins with the background of method used (i.e. microwave method). The properties of ZnO especially on the hexagonal wurtzite crystal structure are discussed since ZnO synthesized in this work has hexagonal structures as confirmed by the characterizations. Besides, the properties of TiO₂ (for Part I), GO, and rGO are also discussed. This chapter ends with the setup and mechanism of photocatalysis and photoelectrochemical reaction (cyclic voltammetry and photocurrent).

Chapter 3: Experimental methods

In this chapter, sources of material and method used are introduced and all the experimental steps are presented. This chapter has three sections; experimental, application methods and characterization techniques. Experimental and application method sections are divided into Part I and Part II of this research work. This chapter ends with the characterization techniques involved in this work.

Chapter 4: Results and discussion

This chapter consists of results and discussion obtained from different characterization techniques covering three categories; structural, optical, and morphological characterization, and also from photocatalysis and photoelectrochemical experiments. This chapter is also divided into two parts; I and II. Part I explains about the comparison between the behavior of commercial ZnO and P25, and Part II focuses on the performance of synthesized samples.

Chapter 5: Conclusions and future works

The results obtained with a review on the objectives of this work are concluded in this chapter. Finally, suggestions of future studies in utilizing the synthesized samples are discussed.

CHAPTER 2 : LITERATURE REVIEW

2.1 Introduction

In this chapter, several topics related to the photocatalysis process will be introduced. It begins with the theory and mechanism of microwave heating method. The history and properties materials such as ZnO, graphene, graphene oxide (GO) and reduced graphene oxide (rGO) are presented next. Brief explanation of TiO₂ is also included as a comparison to ZnO in terms of photocatalytic activity. Followed by the explanation of photocatalytic degradation of methylene blue (MB) by the ZnO and the enhancement of degradation by ZnO/rGO nanocomposites are discussed in detail. Finally, a technique based on the electrochemical is reviewed.

2.2 Microwave

Microwave possesses a wavelength located between infrared and radiowave in electromagnetic spectrum. It is non-ionizing radiation and is defined in a measurement of frequency ranging from 300 MHz to 300 GHz which coincide with wavelength in the range of 1 mm to 1 m. Microwave composed of different sub-bands; L-, C-, X-, and Ku-bands which are used for different applications. Generally, microwave with longer wavelength is used for technology and communication purpose while microwave with shorter wavelength is used for heating purpose (National Aeronautics and Space Administration, 2010).

Heating via microwave technique had been used until now by researches as one of heating methods in chemistry synthesis. This technique benefits researchers by providing several advantages over the conventional heating techniques (i.e. oil bath, hydrothermal, stream bath etc.). The most prominent advantage is fast reaction mixture. In this matter, it could greatly reduce the reaction time from days to hours or even minutes, which significantly could save energy and low operating cost. Thus, it allows a better process control during synthesis process. Other than that, this technique provides even heating to the reaction, and saving

environmental heat loss. The sample heated in microwave will not experience heat conduction as microwave waves could penetrate through the sample from all directions, thus provide uniform heating. However, microwave method still has disadvantage as this method cannot synthesis sample in a very high yield (Kappe et al., 2009).

2.2.1 Principle

Heating in microwave occur when there is interaction between the charge particles of the reaction that being heated with the frequency of microwave radiation generated by magnetron. When microwave at the right frequency radiate the sample, dipoles or ions of the sample will rotate at the same frequency and collides each other producing heat (Liu & Zhang, 2009). The reaction heated using microwave follow by either two mechanisms;

(i) Dipolar polarization

It occurs when polar molecules that possess dipole moment try to align themselves with the applied electric field by rotation. As the molecules rotate, they will re-orientate and collide among themselves. The alignment is depends on the ability of the dipole to respond to the different frequency of the applied field. As the dipoles rotate to align themselves with the changing field, there will be a phase difference between the orientation of the dipole and the field. This phase difference causes energy to be lost, giving rise to dielectric heating (Ambro & Orel, 2011).



Figure 2.1 Dipolar rotation (Tierney & Westman, 2001)

(ii) Ionic conduction

The heat generated by this mechanism due to the presence ions from the dissolved charge particles that move under the influence of electric field. The electric field causes the ions oscillates resulting in an electric current. Then, the induced electric current will heat the reaction due to electrical resistance (Whittaker, 1997). The effect by ionic conductivity is much stronger than the dipolar rotation in term of the heat-generating capacity. The samples containing ions are heated more efficiently than just polar solvents.

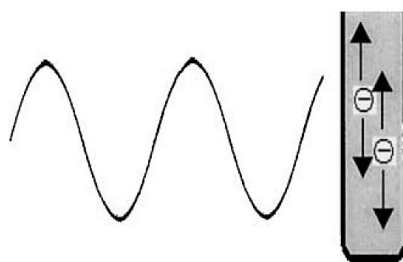


Figure 2.2 Ionic conduction (Tierney & Westman, 2001)

The difference between microwave heating and conventional heating are enlisted in Table 1.

Table 1 Differences between microwave and conventional heating technique (Kappe et al., 2009)

Microwave heating	Conventional heating
The core of reaction mixture is heated directly	The heating starts from the outside of reaction vessel towards inside of reaction vessels and finally to reacting species
Need physical contact between the vessel and the surface source. The vessel is placed in the microwave cavity during heating	Need physical contact between the vessel and the surface source. E.g. autoclave.
The heating start from electromagnetic wave radiation	The heating comes from thermal or electric source
High heating rate	Less heating rate
Heating mechanism involves two principal; conduction and dipolar polarization	Heating mechanism only involves conduction
Selective heating to specific component in reaction mixture	Equal heating to all compound in mixture

2.3 Zinc oxide (ZnO)

ZnO is an n-type semiconductor and was classes as II-VI semiconductor group. Physically, it is a white powder and insoluble in water. It has a wide range of nanostructures among other semiconductors such as nanoflakes, nanorod, nanobelts, and etc. depends on the method used and other controlled parameters during synthesis process (Wang, 2004).

ZnO crystal lattice can be organized into three different phases; cubic rock salt (metastable at relatively high pressure ~ 10 GPa), cubic zinc blende (metastable by means of growth on cubic structure substrates), and hexagonal wurtzite (the most stable at low pressure). However, at ambient pressure and temperature, ZnO thermodynamically tends to crystallize to hexagonal wurtzite over the cubic structure (Hadis Morkoç & Ümit Özgür, 2009).

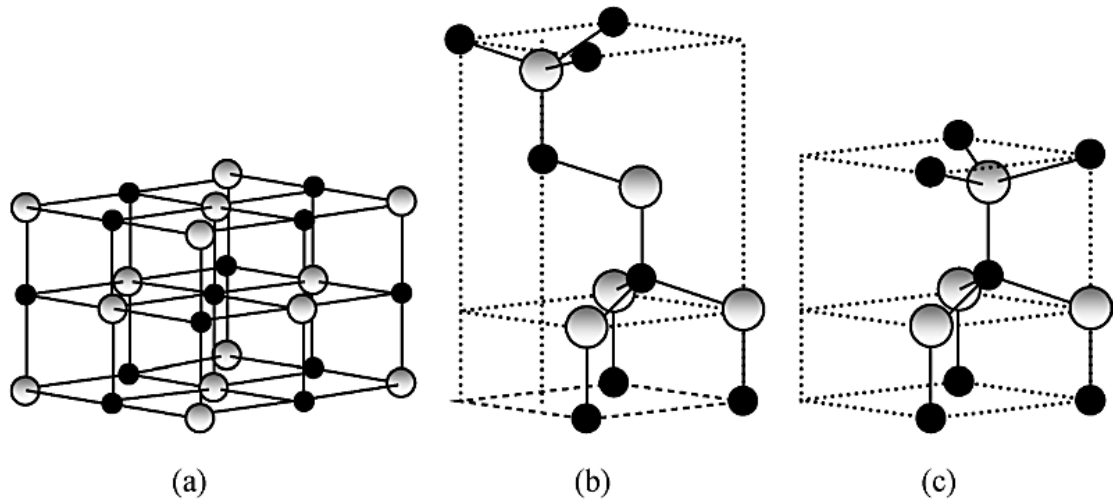


Figure 2.3 ZnO crystal structures; (a) cubic rock salt (b) cubic zinc blende, and (c) hexagonal wurtzite (Hadis Morkoç & Ümit Özgür, 2009)

ZnO in theory has a relatively wide band gap (3.37 eV), high exciton binding energy (60 meV) at room temperature, and has a maximum electron mobility of $\sim 2000 \text{ cm}^2/(\text{V}\cdot\text{s})$ at 80 K, which makes it a suitable material to be used in photonic field (Gusatti et al., 2010). The properties of ZnO depend on the crystal size, morphology and orientation. As grown, it is believed that the conductivity behavior of unintentional n-type ZnO attributed to the presence of native defects such as zinc interstitials or oxygen vacancies. However, the experiment shown that oxygen vacancies act as deep donor and zinc interstitials are too mobile and not stable at room temperature. Given that these defects cannot explain the conductivity of ZnO and the issue was still remained unclear. Until recently, based on theoretical calculations, it was shown that the existence of hydrogen in ZnO act as donors. This was confirmed by experimental techniques that hydrogen is a shallow donor that contributes in the electronic properties of ZnO

(Janotti et al., 2012). Also noted that the band gap energy of every ZnO was not the same due to the different amount of oxygen vacancies that present in ZnO (Liu et al., 2012).

2.3.1 Synthesis and growth mechanisms in alkaline solutions

ZnO nanostructures have been synthesized by various methods, such as hydrothermal, colloidal and sol gel method. As said earlier, ZnO has wide range of nanostructure. Commonly during the growth process, it involves the reaction between Zn salts and hydroxyl ions, forming zinc hydroxide, $Zn(OH)_2$ according to the following reaction mechanism;



Subsequently, $Zn(OH)_2$ produces ZnO seeds as shown by equation below;



The ZnO seeds are the building blocks for ZnO particles. Temperature, pH, water content, ratio of Zn^{2+} and OH^{-} and reaction time are important parameter to control to get uniform morphology and chemical stability of the ZnO particles (Xu et al., 2008).

Hexagonal wurzite is characterized by tetrahedrally coordinated zinc ion and oxygen ion that are stacked alternatively via sp^3 covalent bonding along the c-axis. Figure 2.4 illustrates the unit cell of hexagonal ZnO crystal that has two opposite polar terminated faces referred to positively charged (0001)-Zn and negatively charged (000-1)-O. These polar faces have different chemical and physical properties resulting in the creation of dipole moment, spontaneous polarization orienting along c-axis and a divergence in surface energy. The chemical activities happen at these polar faces causes formation of different type of ZnO nanostructures. Besides polar faces, there are also non-polar faces observed referred to (11-20) and (10-10) which have equal number of Zn and O atoms (Gao & Wang, 2005). Generally, the lattice parameters of ZnO hexagonal unit cell are $a=3.2495 \text{ \AA}$ and $c=5.2069 \text{ \AA}$ with the density of 5.605 g cm^{-3} .

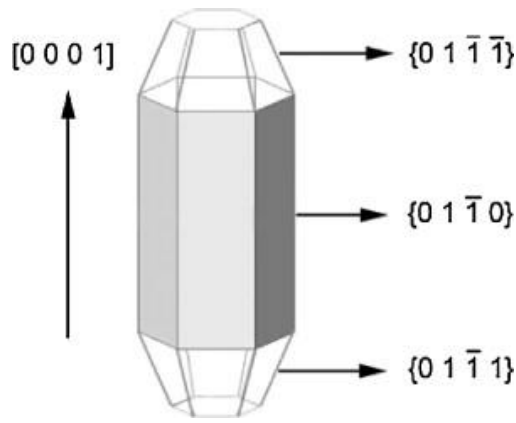


Figure 2.4 Growth habits of ZnO nanoparticles (Bai et al., 2011)

2.4 Titanium dioxide (TiO₂)

TiO₂ is a semiconductor that crystallizes into three naturally existing polymorphs; anatase, rutile and brookite. Anatase and rutile are the common phases have been conducted in experiments. Anatase phase with high specific surface area (BET) shows good photocatalytic activity due to low combination rate of photogenerated electron-hole pairs and more reactive site are created on TiO₂ surface (Pillai et al., 2007).

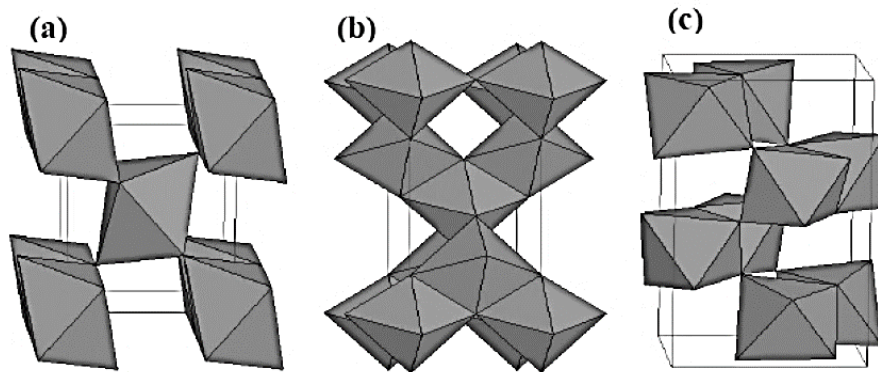


Figure 2.5 Crystal structure of (a) rutile (b) anatase (c) brookite (Freitas et al., 2013)

2.4.1 Comparison between ZnO and TiO₂ in photocatalysis

Even though TiO₂ is known as a good photocatalyst for pollutant degradation due to its photosensitivity, stability, abundant and low cost, ZnO has been considered as an alternative to TiO₂. ZnO is more advantageous than TiO₂ for solar applications because the studies have

confirmed that ZnO show greater activity under sunlight irradiation due to its ability to absorb more light quanta attributed to the existence of vacant anionic site on ZnO surface. In contrast, TiO₂ absorb UV light and is not significantly active under visible light irradiation (Ali et al., 2010).

2.5 Graphene

Graphene is a single sheet of bulk graphite (three-dimensional carbon based material composed of loosely stacked graphene layers) at only one atom thickness. It consists of two-dimensional of sp^2 carbon bonding that are arranged in a honeycomb lattice (Choi et al., 2010).

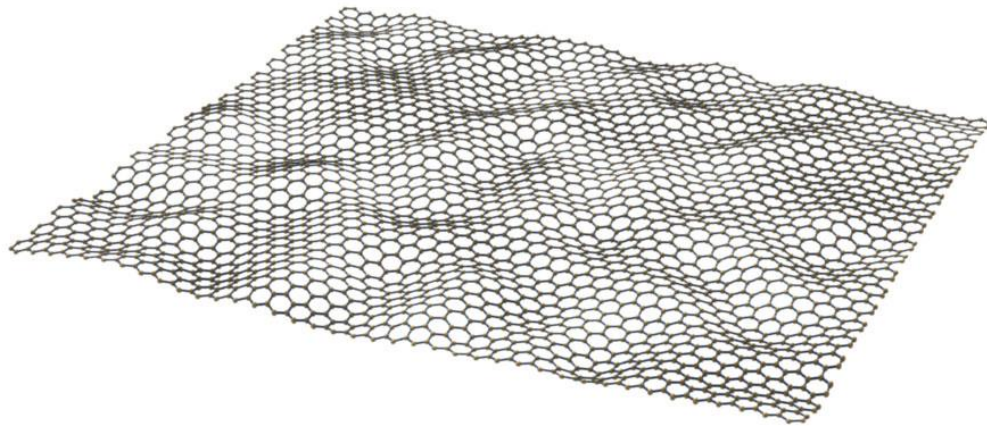


Figure 2.6 Graphene structure (Hedberg, 2013)

The lattice structure of ideal graphene consists of two equivalent carbon atoms A and B per unit cell, with a carbon distance of 0.142 nm. Each atom is bonded to three nearest atoms via strong σ bonds and the bonds are separated by 120°. Carbon atom has four valence electrons in electron shell. Due to strong nature of σ bonds, the electrons do not contribute to conductivity significantly. Three electrons are involved in covalent bond, another one electron may be mobilized from the electron shell, occupies π orbital which allows the electrons delocalized between all carbon atoms within the graphene plane. This contributes to graphene conductivity when there is electric field applied. Graphene layers are attracted by weak Van der Waals force within graphite which allows the layers to separate (Hasan, 2012).

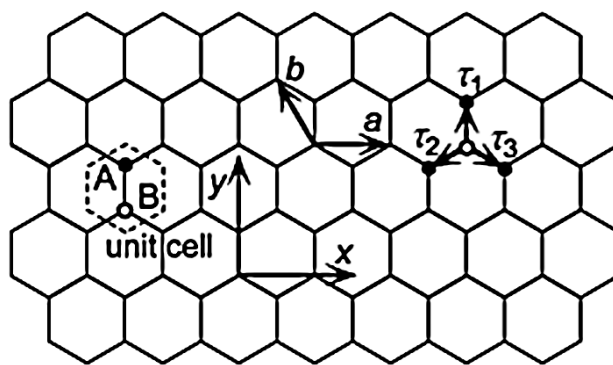


Figure 2.7 Unit cell of graphene (Hatsugai, 2010)

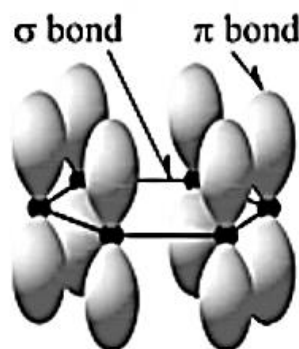


Figure 2.8 Formation of σ bond and π orbital in graphene (Srivastava, 2012)

For ideal graphene, it has almost zero band gap and high electron mobility. To date, many possible techniques have been reported in order to produce graphene in large quantities including chemical vapor deposition (CVD), liquid phase exfoliation of graphite, epitaxial growth on silicon carbide, growth from metal-carbon melts, reduction of carbon dioxide and chemical reduction of graphene oxide (GO). However, chemical reduction by using graphite oxide as precursor appears to be the most promising route towards the large scale production even though this method usually results reduced graphene oxide (rGO), not graphene.

2.6 Graphite oxide/graphene oxide (GO)

Graphite oxide is a compound that contains abundant oxygen functional groups; epoxy (-O-) and hydroxyl (-OH) groups located at basal planes, and carbonyl (-CHO) and carboxyl (-COOH) groups located at the edges, resulting in polar surface properties. Graphite oxide is thermally unstable due to the presence of oxygen functional groups attached to it.

Because of the presence of COOH groups, graphite oxide is hydrophilic that could be easily dispersed in water forming colloid solution (Ganguly et al., 2011).

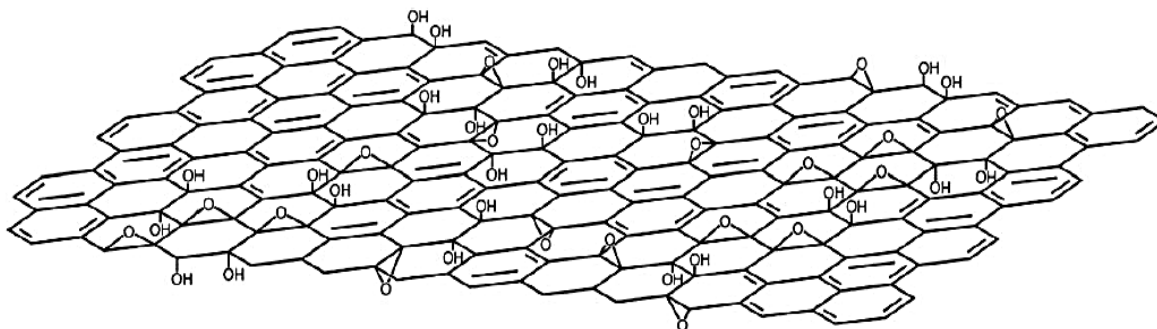


Figure 2.9 Chemical structure of graphene oxide (Park & Ruoff, 2009)

The most common method to synthesize graphite oxide is called Hummers method. This method involves the oxidation of graphite flakes with strong oxidizers in acid environment. The interplanar distance between the graphite layers will increase when it is oxidized. The degree of the oxidation depends on the reaction conditions and the precursor graphite used. Note that graphene oxide (GO) is formed through complete exfoliation of graphite oxide by sonication or vigorously stirred in water for a long enough time. However, there is no difference between graphite oxide or GO in terms of composition. Thus, it is common to refer the graphite oxide as GO. During the oxidation process, the increased of interplanar distance disrupts graphite's sp^2 bonding network causes non-conductivity of GO (Stone, 1988). Oxygen react to different sites on the graphite sheets and may attach to adjacent carbon on the surface. This reaction causes to the weakening of the Van der Waals interaction between the graphene layers. The π conjugated structure and electrical conductivity of GO can be healed to the level of graphite through a controlled process of deoxidation by restoring carbon network through chemical reduction (Marcano et al., 2010).

2.7 Reduced graphene oxide (rGO)

rGO is a graphene-like structure that provides high surface area, thin layer, and conductivity. Thermally reducing GO at very high temperature would affect the structure of graphene platelet due to pressure that builds up between the platelet and release of carbon

dioxide. This would create imperfections and vacancies at rGO. rGO is widely produced through chemical reduction of GO for high yield production. However, synthesized rGO through this method still results poor crystallinity and electronic conductivity as compare to graphene due to the oxygenated functional groups that still remain and formation of lattice defects after reduction. Despite its poor quality, this does not mean rGO is effectively unusable. By considering for large scale production for industrial application, rGO is the significant solution (Fuente, 2013).

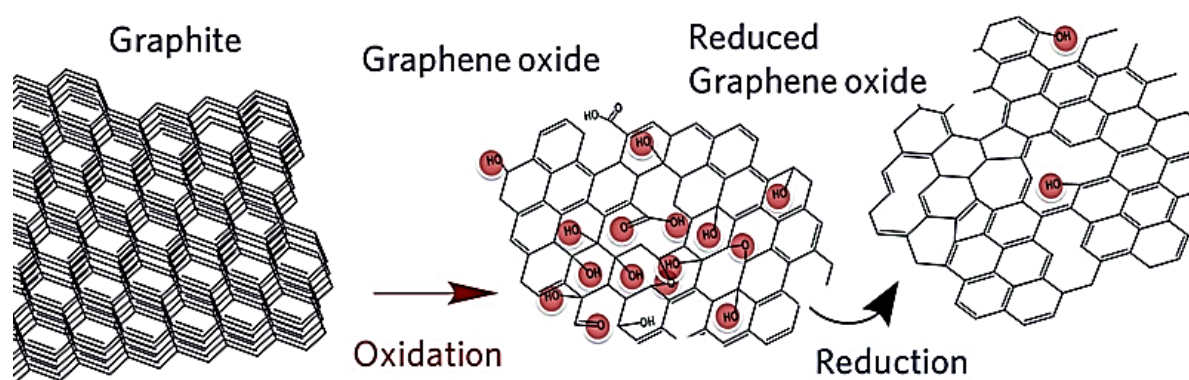


Figure 2.10 Schematic mechanism of oxidation of graphite producing GO and chemical reduction of GO producing rGO (Kauppila & Viinikanoja, 2012)

2.8 Zinc oxide/reduced graphene oxide (ZnO/rGO) nanocomposites

Due to useful properties offers by rGO, various methods have been applied to prepare rGO, and one of the possible method was incorporating rGO with other materials forming composite materials. Composite can be defined as a combination of two or more individual components with different properties, forming a final material with different characteristic from the individual component (Olad, 1996).

ZnO atoms have a greater tendency to agglomerate arises from their surface energy. If the atoms agglomerate, they can form one large particle, resulting lower performance in applications. GO have oxygenated functional groups that act as anchor sites for deposition and nucleation of particles, and consequently make ZnO particles formed on the surfaces and edges of rGO sheets. Large surface area of rGO can act as a ZnO support. Note that, the rGO sheets

may be recombined due to Vander Waals interaction between the sheets. Therefore, by combining rGO with ZnO, it is helpful in overcoming this interaction. The crystallization of ZnO on the rGO surface could prevent the agglomeration of ZnO and simultaneously could prevent the restacking the rGO sheet (Xu et al., 2011).

Briefly, the synthesis of rGO-supported ZnO started with the oxidation of graphite forming GO followed by exfoliation of GO via sonication in water. At this stage, the interplanar space of exfoliated GO become larger. When the zinc source mix with GO, there will be an interaction between Zn^{2+} and oxygenated group of GO in the presence of reducing agent. During the heating treatment, the GO will be deoxygenated and simultaneously nucleation of ZnO particle occurs forming rGO/ZnO nanocomposite (Lim et al., 2012). A schematic mechanism for decorating ZnO nanoparticles onto rGO sheets is shown in Figure 2.11.

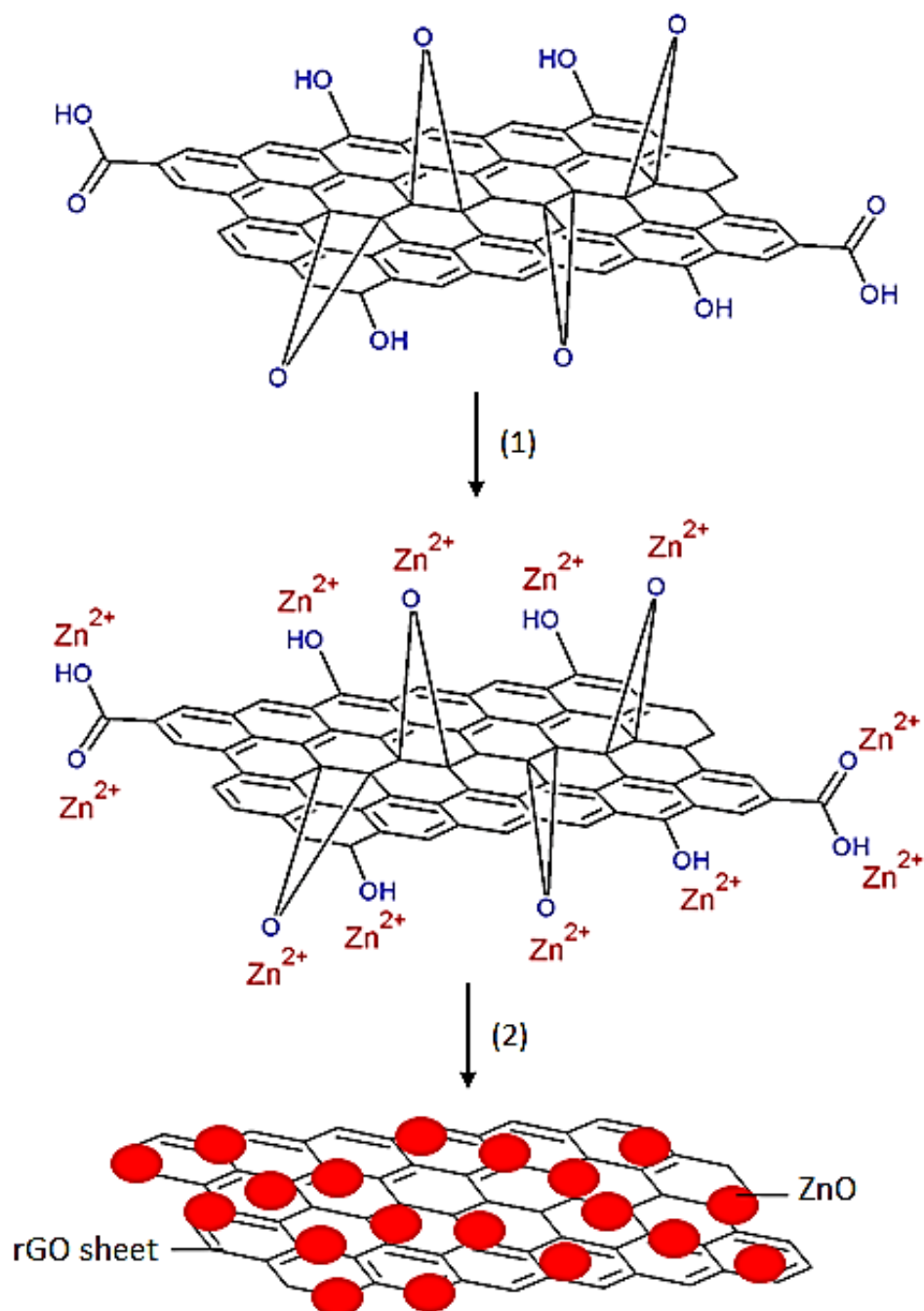


Figure 2.11 A proposed schematic route for decorating ZnO onto rGO sheets. (1) Interaction of Zn ion with the oxygenated group of GO. (2) Formation of ZnO/rGO composite

2.9 Diethylenetriamine

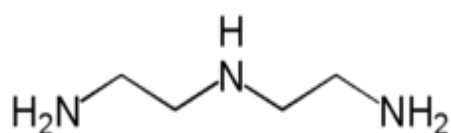
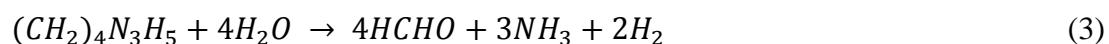


Figure 2.12 Chemical structure of Diethylenetriamine

Diethylenetriamine (DETA) is a water-soluble tridentate amine that has the chemical designation N-(2-aminoethyl-1, 2-ethanediamine). DETA can act as a hydrolysis agent as it can react with water and OH⁻ due to equilibrium process. It plays a role as a stabilizer as well as structure directing agent to control the morphology of the samples. During synthesis with zinc source, it coordinates the Zn²⁺ forming zinc-amine complex. The reaction can be expressed as below (Yi et al., 2008);



2.10 Heterogeneous photocatalysis

Photocatalysis is a photochemical reaction that occurs in the presence of catalyst through light absorption. Unlike metal which has an overlap of valence band (VB) and conduction band (CB), semiconductor has an energy region to separate the CB and VB where no electron states are allowed in this region. Photocatalytic activity depends on the ability of semiconductor photocatalyst to generate electron and hole pairs, and excite the electrons across the band gap in the presence of light. The generated charges are responsible to initiate reduction-oxidation (redox) process and involve in transformation of the reaction partners. Radicals will be produced and leading to the mineralization of organic pollutants. Besides keeping the environment clean, this treatment is considered as economical operation due to this process does not need other consumable chemicals and able to work at very low contaminant concentration since pollutant is attracted strongly to the surface of photocatalyst (Al-Rasheed, 2005).

2.10.1 Methylene blue

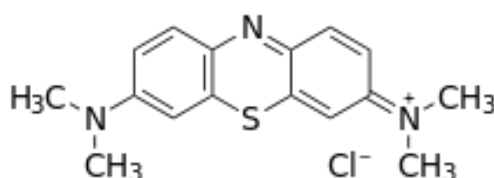


Figure 2.13 Chemical structure of methylene blue (Adams et al., 2007)



Figure 2.14 Methylene blue solution

Methylene blue (MB) is an aromatic compound with the chemical formula $C_{16}H_{18}N_3SCl$ that commonly used as dye pigment in textile industry, as an indicator and even used in medical treatment. It is hydrophilic cationic dye that appears blue when dissolved in water and has maximum absorption of light of 663 nm. It is chemically inert, stable in water and toxic that causes damages to ecosystem in water, human health and surrounding environment. In photocatalysis, MB is popular organic compound that used as test pollutant. When it is under go photodegradation by photocatalyst upon illumination, it appears colourless (Soltani et al., 2012).

2.10.2 Photocatalytic properties of ZnO/rGO nanocomposite

Due to the stability of MB in water, it is not easy to be removed. Advance Oxidation Process (AOP) is a suitable method to decompose the MB dye; by using activated hydroxyl radical reaction (Kasiri & Khataee, 2011). In photodegradation of dye, the degradation by ZnO occurs together with the excitation of dye. Upon illumination of light that has energy of $h\nu$ equal to or larger than the band-gap energy of ZnO, the incident photon will be absorbed by ZnO. Electrons with enough energy will excite across the band-gap energy to conduction band (CB) and leaving behind holes at valence band (VB). At the same time, electrons from the dye will be excited to the CB of ZnO, thereby generating extra electrons. The reaction continue with the separated charges migrate to the ZnO surface, and react with the adsorbed species through redox reaction. Electrons react with oxygen and generate superoxide radical anion ($O_2^{\bullet-}$). This stage is also called as electron scavengers which play role to extend the duration of the charges recombination. While holes react with surface-bound H_2O and generate the hydroxyl radicals (OH^{\bullet}). The generated radicals will subsequently degrade the dye molecule to clear solution. The proposed mechanism is described briefly in the equations below (Colmenares et al., 2009);

1) Absorption of light ($E \geq E_g$) by ZnO and generating electron and hole pairs



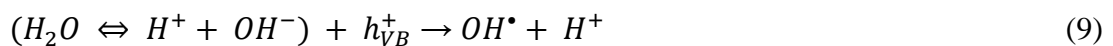
2) Electron trapping



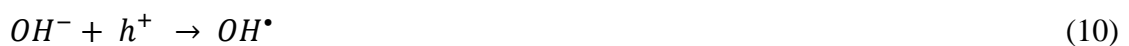
3) Electron scavenging



4) Formation of OH^{\bullet} by holes



5) Oxidation of hydrolysis



6) Photodegradation of dye molecule (R) by hydroxyl radicals



7) Direct oxidation by holes



$O_2^{\bullet-}$ will further react with H^{+} to form hydroperoxyl radical, HOO^{\bullet} which could doubly extend the duration of the recombination from occur during the photocatalysis process.

However, photodegradation of dye by ZnO under visible light may not efficient and typically shows low photocatalytic activity. This is due to fast recombination of the generated charges and it requires high energy of light irradiation since it has wide band gap. Obviously, the separation and recombination of charges between ZnO and dye greatly influence the photodegradation efficiency. Therefore, modification to the ZnO should be done to have visible light catalytic activity, thereby enhancing the photocatalytic activity. Here is when the rGO is needed in order to improve the photodegradation rate. It is suggested that when rGO is introduced into ZnO, there will be an electronic interaction between rGO and ZnO that would narrow the band gap of ZnO and enlarge the light absorption range (Yeh et. al, 2013). Besides that, very high electron mobility that offered by rGO makes it able to accept and transport electrons in preventing the recombination of the charges within ZnO. Finally, the interaction between ZnO and rGO increases the interaction area and adsorption of dye molecules through π - π interaction (Li & Cao, 2011).

There are two mechanisms have been proposed by researchers for the ZnO/rGO composite mediated dye photodegradation process;

- (i) The excitation of electrons from VB to CB of ZnO when irradiated with suitable light energy. The movement of separated charges towards the ZnO surface forming active oxygen species, and the reaction with the dye molecules takes place. This mechanism is based on the band gap energy of the ZnO (Narayan et. al., 2009).

(ii) The adsorbed dye at ZnO particles is photochemically excited when irradiated with visible light (as dye molecules absorb in the visible regions) and transfer electrons to the CB of ZnO through rGO. At the same time, the dye becomes a cationic radical leads to degradation of other dye molecules and self-degrades. This mechanism is based on the amount of effective surface area provided from the small size of ZnO particles and referred to as photosensitization process (Narayan et. al., 2009).

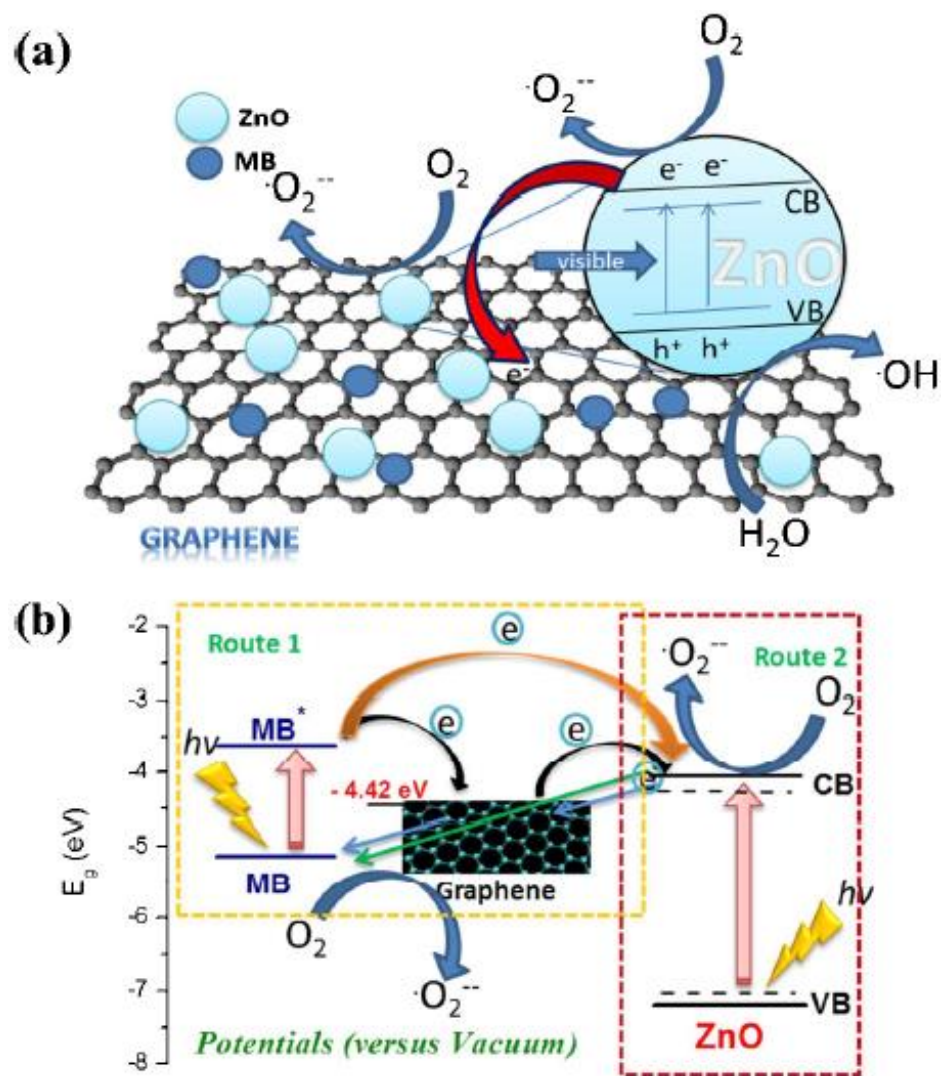


Figure 2.15 Two proposed mechanisms of photocatalytic activity of MB by ZnO/rGO composite (Adán-Más & Wei, 2013)

2.11 Photoelectrochemical processes

The mechanism of photoelectrochemical process is the same as photocatalysis, which need separation of the charges when illuminated with light. The different is for photoelectrochemical, a potential is applied to the reaction using potentiostat. The photoelectrochemical reaction depends on the optical properties and also the nature of the illuminated sample. The setup needs solar light, electrochemical cell and electrodes where the photocatalyst must be in contact with working electrode for allowing the photogenerated electrons to flow through the reaction circuit.

2.12 Photoelectrochemical measurement

Photoelectrochemical setup consists of light source, potentiostat, cell, and three electrodes including working, reference and counter electrode. Table below shows the function of different component involved during photoelectrochemical experiment.

Table 2 Function of electrochemical components (Gamry Instruments, 2013)

Component	Function
Potentiostat	An electronic tool to control the potential of counter electrode against working electrode.
Working electrode (WE)	The electrode that can measures current and serves as a surface on which the electrochemical reaction is happening. There are different types of working electrode that are usually used such as are metals, carbon-based, film electrode and etc. The redox process between the sample and the analyte can be studied at the surface of this electrode.

Reference electrode (RE)	The electrode that used as a reference for controlling and measuring potential between the working electrode and electrolyte. This electrode should hold a constant potential during testing to obtain good electrochemical data. This can be achieved by having no current flow through it, or if some current does, the potential will not be affected. Example of reference electrode which is commonly used are silver/silver chloride (Ag/AgCl), saturated calomel electrode (SCE), and mercury/mercury sulfate (Hg/Hg ₂ SO ₄).
Counter electrode (CE)	The electrode that completes the electrical current path in the electrochemical cell by conducting current leaves electrolyte. It is typically made of inert material such as platinum, carbon, graphite etc.
Cell	That container that filled up with electrolyte solution

There are four main factors that contribute to the efficiency of the photoelectrochemical reaction such as material used to form film at working electrode, film thickness, light intensity, and type and concentration of electrolyte. Electrolyte solution is an ionized solution that can conduct electricity due to the movement of positive and negative ions that present in the solution. The higher the concentration of electrolyte, the higher the conductivity, thereby lowers resistance.

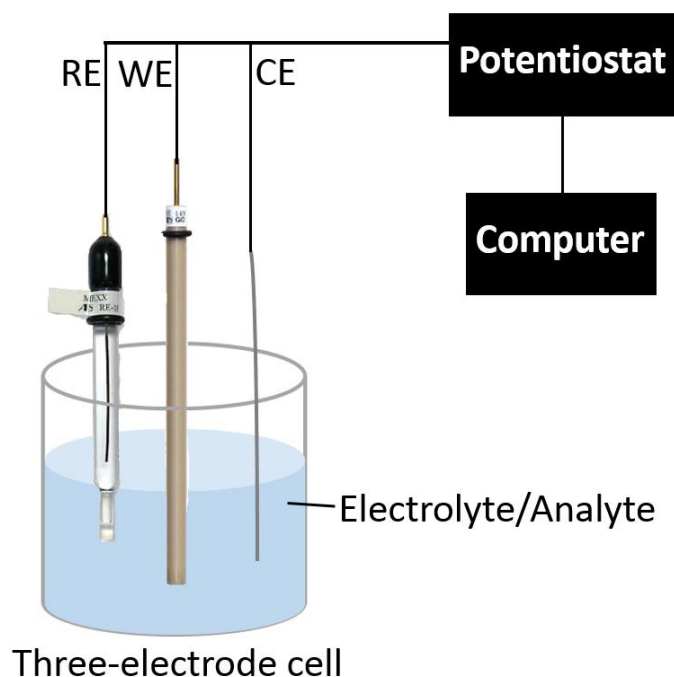


Figure 2.16 Schematic diagram of a conventional three-electrode cell

2.13 Cyclic Voltammetry (CV)

CV is one of electrochemical techniques that usually be used to deal with any electrochemically active species. It measures the current that arises at the electrode surface by adjusting the potential in the electrochemical reaction. CV is widely used by researchers for variety of applications such as to study concentration of analyte, the stability of sample towards redox processes of analyte, adsorption and diffusion processes occur on electrode surface, electron transfer mechanism for energy levels studies and also for detection for electrochemical sensor applications.

Figure 2.17 shows the triangular voltage waveform that is applied to the working electrode. In CV, the voltage is swept between two potential values, V_1 and V_2 . When the voltage from V_1 reaches V_2 , the ramp will reversed and bring the voltage back to V_1 .

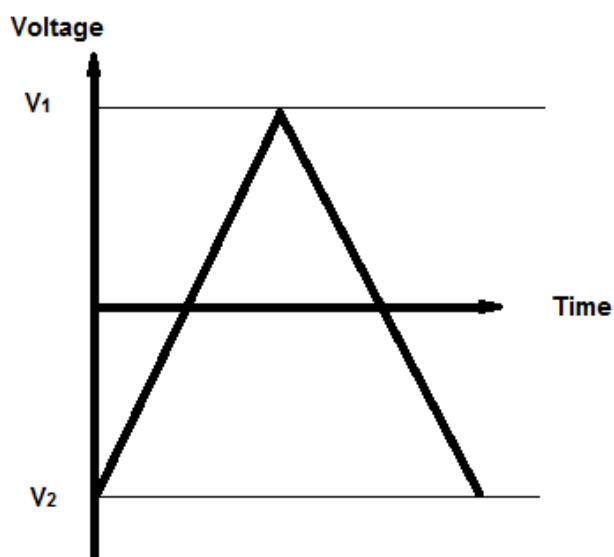


Figure 2.17 Cyclic voltammetry voltage sweep (Gouws, 2012)

A typical graph of current (I) versus voltage (E) known as cyclic voltammogram is shown in Figure 2.18. The oxidation and reduction occur between two potential values. The potential can be fixed dependence on the properties of analyte that can be oxidized or reduced within the experimental potential window. Point A, B and C describe the cathodic side. From point A, when the voltage is applied, an amount of current is increased indicates analyte is reduced. The peak current (i_p) increases until reaches maximum amount at point C. After point C, the voltage is still applied but the current decreases due to a depletion of analyte molecules. Point D, E and F describe the anodic side where the reverse process occurs. Here is when the voltage applied decreased, the analyte is oxidized and return back to its initial state. The intensity of the peak observed is proportional to the concentration of analyte at the electrode surface (Jay, 2014).

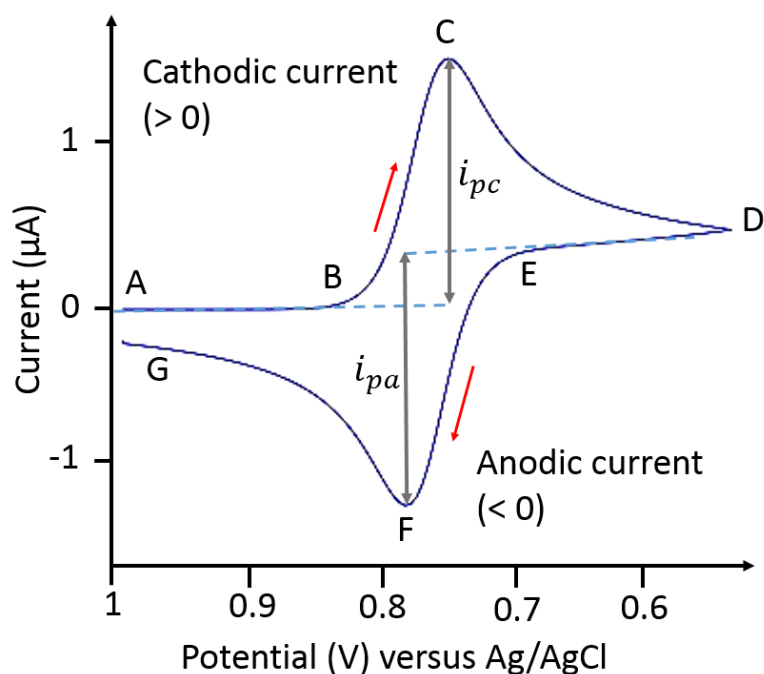


Figure 2.18 Typical cyclic voltammogram

2.14 Photocurrent

Photocurrent is another valuable measurement employed in electrochemical technique. Photocurrent measurement dealing with heterogenous charges transportation and it was first reported by Marecek et al. It provides information about the charges transportation and recombination, and the chemical reactions happening at the photoelectrode/electrolyte interface during light illumination. Driving force is applied to separate the photogenerated charges, and consequently, photocurrent response produced. The photocurrent response increases if the density of free carrier increased when illuminated by the light. The photocurrent reading will decay to the original value (dark current) when the reaction is blocked from illumination. In this research, photocurrent measurement can be linked to the photocatalysis by providing evidence of photoinduced electrons transportation during solar light illumination (Compton, 1989).

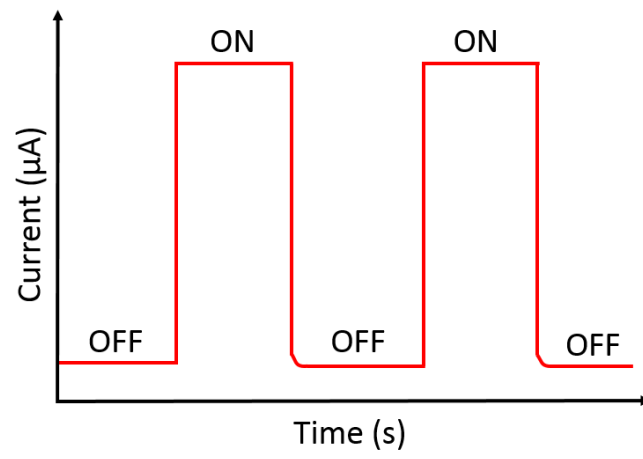


Figure 2.19 Typical photocurrent graph

CHAPTER 3 : EXPERIMENTAL METHODS

3.1 Introduction

In the early part of this chapter, the list of source of materials used in this work is stated, followed by the experimental, application methods, and characterization techniques section. Under the experimental section, it is divided into two parts. The first part covers for the preparation of commercial ZnO and Degussa TiO (P25) photocatalyst in powder form and in immobilized form. This is done to compare the performance between commercial ZnO and P25 photocatalyst. The second part covers the preparation of the synthesized samples which are ZnO, GO and ZnO/rGO nanocomposites. Next is application methods section which is also divided into two parts. First part is application for commercial ZnO and P25 photocatalyst and the second part is for the synthesized samples. Under this section, the photocatalysis and photoelectrochemical experiment are demonstrated. Finally explanation on characterization techniques used for photocatalyst analysis is explained.

3.2 Part I

3.2.1 Materials

Commercial ZnO and P25 were purchased from Acros Organics and methylene blue (MB) was purchased from System. Deionized water (resistivity $\geq 18\text{M}\Omega$) was used throughout the experimental process.

3.2.2 Experimental

Commercial pure ZnO was mixed with distilled water to produce slurry form. Then the slurry was applied onto a glass slide using doctor's blade method to produce immobilized ZnO. The coating dimension was fixed at 4 cm x 2 cm with a mass of 12 mg. To make the photocatalyst stick well on the glass slide, the coating was calcined using furnace at 450°C for

2 hours. The steps were repeated for P25. The stability of the coating was tested by immersing the immobilized photocatalyst in the stirred water for three days, and no floatation of photocatalyst observed. Then for preparation of powder photocatalyst, the same mass and calcination parameters were employed.

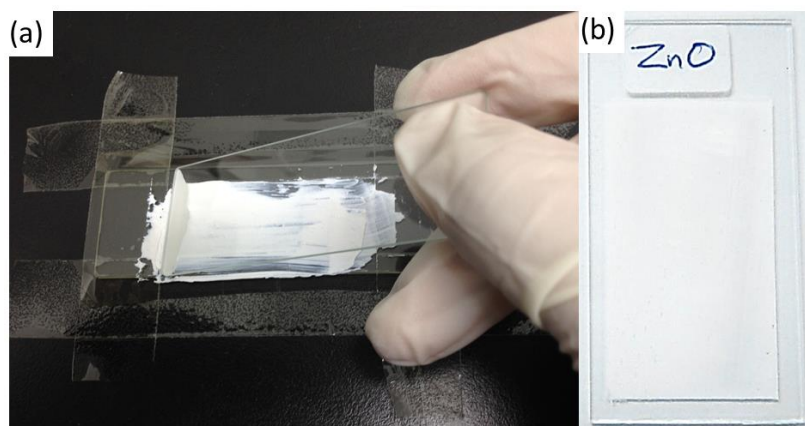


Figure 3.1 (a) Preparation of immobilized photocatalyst before calcination
(b) Immobilized photocatalyst after calcination

3.2.3 Application methods

3.2.3.1 Photocatalytic activity test

For UV light irradiation, the immobilized photocatalysts; ZnO and P25, were put in a beaker containing 100 ml of 1.5 ppm MB solution and placed inside Ultraviolet Crosslinker (UVP-CL-1000, Cambridge) with $5800 \mu\text{W}/\text{cm}^2$ intensity. Prior photocatalytic test, the reactions were magnetically stirred in the dark to reach adsorption-desorption equilibrium between the photocatalysts and MB solution. The Ultraviolet Crosslinker was then stacked on top of the hotplate to stir the reactions during irradiation. The irradiation was run for 30 min and the distance between the light source and the reaction was fixed 13 cm apart. The setup was repeated for suspension photocatalysts. The test was repeated for solar irradiation which the light is provided by solar simulator Oriel Instrument (Newport Corporation, Irvine, CA, USA) with irradiant of 100 mW cm^{-2} using 150 W xenon light source (AM 1.5 G). The reaction in the absence of photocatalyst was also performed for both irradiations as a control.

3.2.3.2 Cyclic voltammetry experiment

The experiment were run using a VersaSTAT 3 potentiostat (Ametek Princeton Applied Research, Oak Ridge, TN) with a conventional three-electrode cell (working electrode: the modified glass carbon electrode (GCE) (3 mm diameter, Princeton Applied Research), reference electrode: an Ag/AgCl (in saturated 3 M KCl) and counter electrode: platinum wire). 1.5 ppm MB solution was used as the analyte, and 0.1 M KCl was used as the supporting electrolyte. For preparation of modified GCE, the bare GCE was first polished using 0.1 μM of alumina solution on a micro-cloth polishing pad (Buehler, Lake Bluff, IL) and rinsed with distilled water. Then the polished GCE was tapped onto the photocatalyst powder. Without illumination, the measurement was run at potential range between -1.0 V and 1.0 V with a scan rate 50 mVs^{-1} under cyclic voltammetry mode for 2 hours and the data was taken every 20 minutes throughout the experiment. The measurement with same parameter was repeated by exposing the reaction to solar illumination provided by solar simulator.

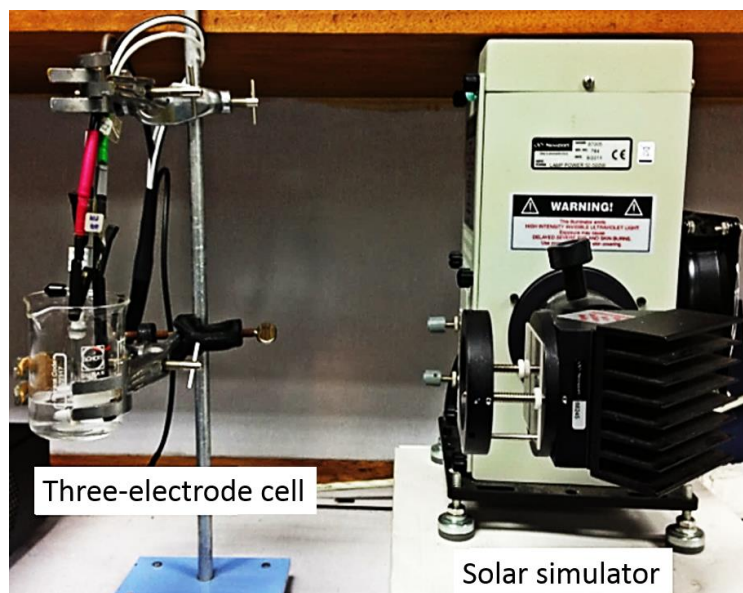


Figure 3.2 Photoelectrochemical setup

3.3 Part II

3.3.1 Material

Graphite 3061 was purchased from Asbury Graphite Mills Inc (Asbury, NJ), diethylenetriamin and potassium permanganate (KMnO_4) were purchased from R&M Chemicals (System, Malaysia). Sulfuric acid (H_2SO_4), phosphoric acid (H_3PO_4), hydrogen peroxide (H_2O_2), and ethanol were purchased from Merck KGaA (Darmstadt, Germany). Deionized water was used throughout the experimental process.

3.3.2 Experimental

3.3.2.1 Synthesis of GO

GO was synthesized using the simplified Hummers method (Hummers & Offeman, 1957; Marcano et al., 2010). 3 grams of graphite flakes was added into a mixture of 9:1 concentrated H_2SO_4 : H_3PO_4 solution (360:40 mL), followed by gradually added 18 grams of KMnO_4 . The mixture was left under magnetic stirring to oxidize. After three days, the color of mixture turned from dark purplish to dark brown. The mixture was then cooled to room temperature and poured into 400 mL ice bath together with 27 mL of 30% H_2O_2 to stop the oxidation. The color is then turned into yellow, showing the graphite oxide is highly oxidized. After the oxidation, the solution was washed and centrifuged with 1 M HCl and DI water for 3 and 10 times, respectively, to remove the unreacted mixture. During the washing process, the graphite oxide is exfoliated causing thickening of GO. Finally, GO gel was obtained.

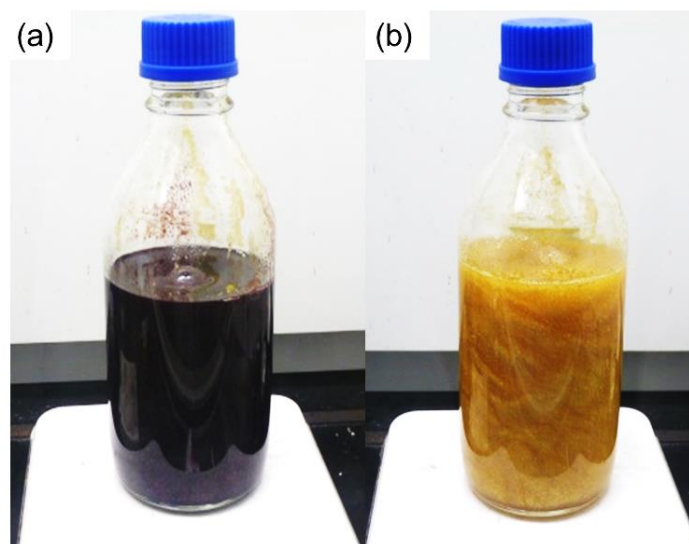


Figure 3.3 The reaction process of Simplified Hummers method (a) before 3 days oxidation (b) after 3 days oxidation



Figure 3.4 Graphene oxide gel

3.3.2.2 Synthesis of ZnO, rGO and rGO/ZnO nanocomposites

The rGO/ZnO was prepared as follows; 20 μL of DETA was added into 4.6 mM $(\text{Zn}(\text{CH}_3\text{COO})_2 \cdot 2\text{H}_2\text{O})$ solution. Then, the zinc solution was slowly dropped with flowing rate of 1 drop/sec followed by 0.09 M NaOH into GO solution until the mixture reached pH 12. The mixture was stirred for 13 hours to obtain homogenous solution. After that, the mixture was transferred inside a household microwave and heated for 30 min. After heated, the solution

was allowed to cool at room temperature, washed and centrifuged with distilled water for three times, to eliminate the residual salt, and dried at 60°C in oven for 24 hours. For composite variation, different amount of GO loading were used; 0.2, 0.7 and 1.5 wt% of GO gel, denoted as ZG3, ZG2 and ZG1, respectively. ZnO and rGO were synthesized using the similar procedure in which for ZnO without GO gel added, and for rGO without zinc source added. For comparison purpose, composite without DETA was also prepared under the same condition and labeled as ZG.



Figure 3.5 Microwave (model: NN-S553WF)

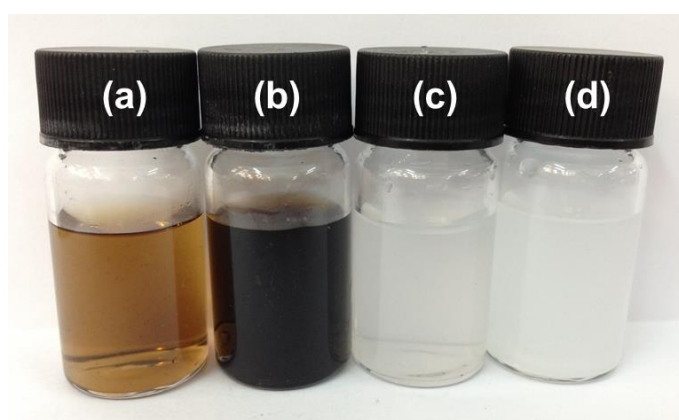


Figure 3.6 (a) GO (b) rGO (c) ZnO in the presence of DETA (d) ZnO in the absence of DETA

3.3.3 Application methods

3.3.3.1 Dark adsorption test

Dark adsorption test was done to distinguish the function of rGO as an absorber and ZnO as a photocatalyst. In this test, 5 mg of each sample was stirred overnight in 240 mL of 5 ppm MB solution without light illumination. This process needed to ensure the MB molecules were totally adsorbed by the samples to reach saturation adsorption. The suspension was then centrifuged and the left MB concentration was measured within 450 nm to 750 nm using the UV-vis spectrometer. By comparing the concentration of MB solution before and after the test, the adsorption rate of the samples could be determined.

3.3.3.2 Photocatalytic activity test

After the dark adsorption test, the same samples were further investigated by monitoring the photodegradation of MB solution. The same samples were used and stirred in 10 mL of 5 ppm MB under natural sunlight for 120 min. Every 20 min, 2 mL of the suspension was withdrawn and centrifuged, and the concentration of MB solution was measured. The best photocatalyst can be determined by analyzing the photodegradation rate of the samples.

3.3.3.3 Cycle test

A valuable feature of the samples is their stability and reuse capability without mechanical failure. Recycling the sample is necessary to know whether the sample can be reused after photocatalysis process. To verify this, the photocatalytic activity test was repeated for six times using the same sample in the same conditions. For every cycle, the sample is washed with DI water to remove attached MB on the surface of the sample, and centrifuged to separate the mixture solution. The separated sample was added again to a fresh identical MB solution. The change of concentration of MB solution between the reuse cycles was recorded and calculated using the formula of C_t/C_0 (C_t : concentration of MB solution at time t ; C_0 : concentration of MB solution at initial time).

3.3.3.4 Photocurrent Measurements

Besides photocatalysis, photocurrent study is done to investigate the interaction between rGO and ZnO by studying the electron transition before and after rGO loading. From this experiment, the data can be correlated with photocatalysis results. In this experiment, it is important to make sure the parameter and condition of working electrode for every sample are same. The working electrode is made by coating the sample onto conductive substrate. 0.5 mg of sample powder was mixed with distilled water to form slurry, then smeared onto a 1 cm x 1 cm indium-tin oxide (ITO) glass using doctor's blade method as shown in Figure 3.1. After that the coated ITO glass was dried in the oven at 60 °C for 24 h.

The experiment were run using a VersaSTAT 3 potentiostat with a conventional three-electrode cell [working electrode: the coated ITO, reference electrode: an Ag/AgCl (in saturated 3 M KCl) and counter electrode: platinum wire]. The light is provided by solar simulator. During the measurement, the solar simulator is switched on and off for every 50 sec and the photoresponse of the samples were measured at 0.5 V under cronoamperometry mode.

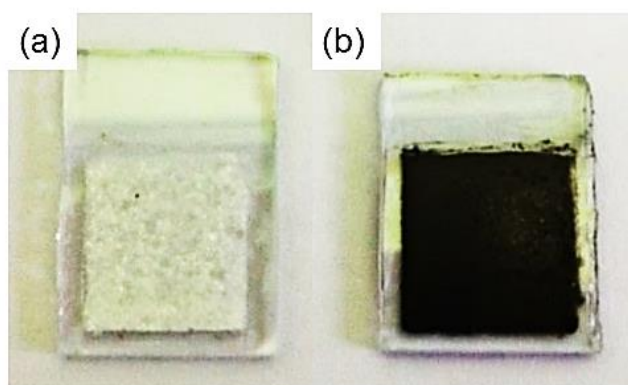


Figure 3.7 Working electrode; (a) ZnO (b) ZnO/rGO nanocomposite coated on ITO glass

3.4 Characterization techniques

After synthesis, the obtained samples were characterized by various characterization techniques to study the crystal structure, optical properties, morphology, size, and element compound.

3.4.1 X-Ray Diffraction (XRD)

XRD technique is used to identify the crystalline structure, d-spacing, orientation and compounds of the sample by analyzing their diffraction patterns. The samples were characterized by X-ray diffractometry (XRD) Siemens D5000 operating at a voltage of 40 kV and a current of 40 A with CuK α radiation ($\lambda=1.4506$ Å). The 2θ scanning range was 5° - 80° with a scanning rate of 0.033°/s. The raw data from XRD measurement is then transferred to PANanalytical X'pert Highscore software to analyze the atomic structure. The orientation of the planes in crystal lattice also can be analyzed by assigning three integers (h k l) known as Miller indices.

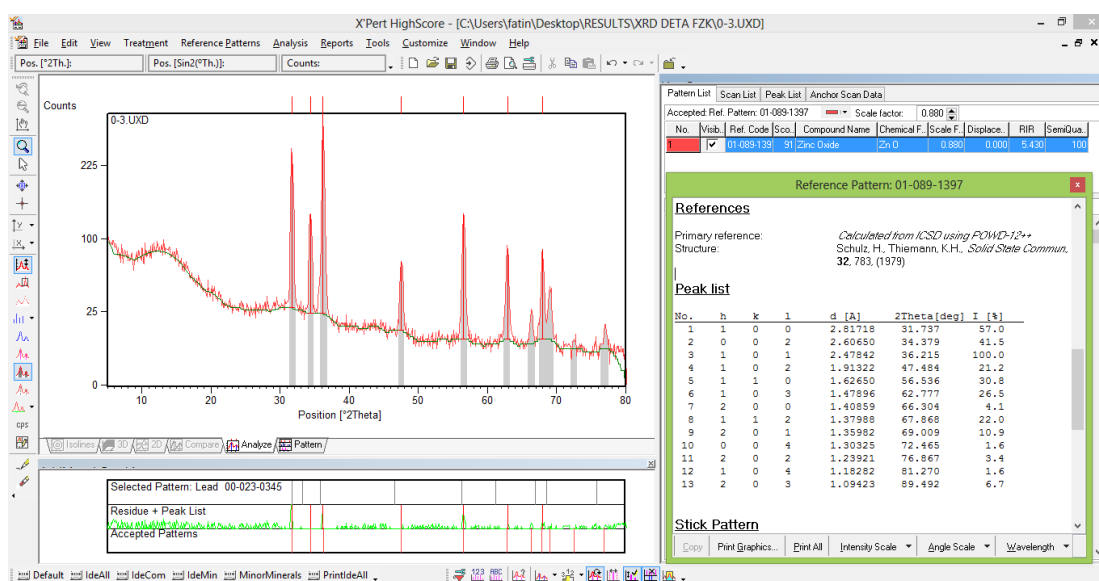


Figure 3.8 Screenshot of PANanalytical X'pert Highscore software

3.4.2 Ultraviolet-Visible (UV-Vis) Spectroscopy

For optical properties, UV-Vis spectroscopy is important technique to study the absorption of light of the sample. The measurements were recorded using UV-vis spectroscopy Thermoscientific Evolution 300 machine which is connected with Thermo Scientific VISIONpro software. In brief, sample powder was sonicated with deionized water to produce sample in solution form. Then, a quartz cuvette containing sample solution and another quartz cuvette containing deionized water which acts as reference were inserted in the cuvette holders.

As beam source, xenon lamp is used to produce beam with a wavelength from 190 nm to 1100 nm. Typically, during the measurement, after the beam splits and pass through the reference and the sample, the detector connected to the software program will detect and manipulate the reference and the sample beam to produce the absorbance spectrum as a function of wavelength. The absorbance of a solution is dependent to the concentration and type of the absorbing species.

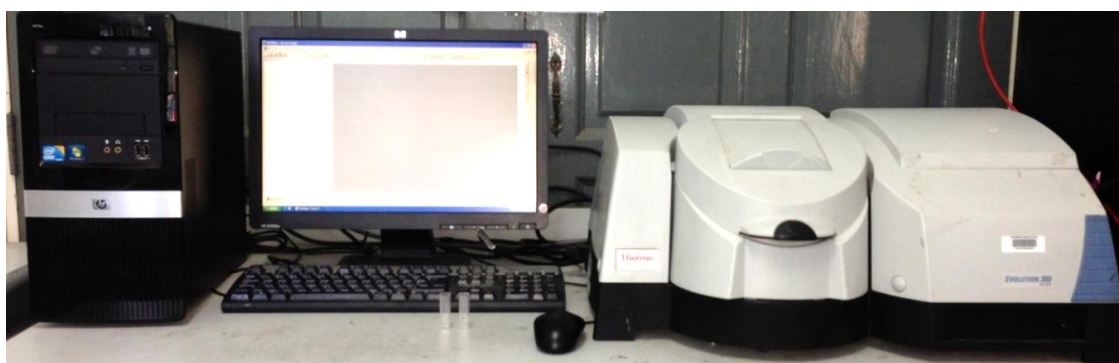


Figure 3.9 Thermo Fisher Scientific Evolution 300 UV-Vis spectrometer

3.4.3 Raman spectroscopy

Raman is a technique to identify the molecular structure of the sample and study its properties by analyzing the vibrational modes of a molecule. The measurements were recorded by using Renishaw inVia raman microscope system, excited with laser power 10% with a wavelength of 514 nm (green laser). The wavenumber was calibrated using the 520.5 cm^{-1} peak of silicon. The measurements were scanned from 200 to 2000 cm^{-1} . Selection of laser is important as it has an impact on experimental capabilities. Wrong selection of laser causes some parts of the sample not be characterized. From the spectrum obtained, the peaks give information about molecular structure of the sample. Other than that, in this research, the crystalline quality of the graphene can be investigated.



Figure 3.10 Renishaw inVia Raman microscope

3.4.4 Field Emission Scanning Electron Microscopy (FESEM)

FESEM characterization is used to visualize the morphology of the entire surface of samples in high resolution. This technique is important in this research work to study the shape of nanoparticles and deposition of ZnO particles on rGO sheet. The morphology of the samples was viewed by using the field-emission scanning electron microscopy (FESEM, JSM-7600F) with an acceleration voltage of 5 kV. Size of ZnO nanoparticles was measured by using ISolution Lite software.

This technique is done in a high vacuum instrument to flow the electron beam to trace over the sample and creating image on a monitor. Specimen for FESEM viewing must be prepared for the high-vacuum environment. The specimen can be prepared by either in powder, film or solution form that is drop-casted onto the silicon wafer. For the sample in solution form, the specimen must be dried before placing the specimen in the FESEM chamber.

For Energy Dispersive X-ray Spectroscopy (EDX) measurement, it must be coupled with FESEM system. EDX is a technique used to identify the elemental composition that present in the sample. The analysis was done at accelerating voltages of 5 kV.

3.4.5 High Resolution Transmission Electron Microscope (HRTEM)

Like FESEM, HRTEM also is used to determine the morphology and particle size. The superiority of HRTEM is that the images can be taken with extremely high resolution until able to measure the lattice of particle. The viewing is recorded using the high resolution transmission electron microscopy (HRTEM, JEM-2100F) with an acceleration voltage of 200 kV.

This technique also is done under vacuum environment. Sample powder has to be prepared in solution form and drop-cast onto a holey copper grid in order to provide sufficient contrast between the sample and the background. The solution need to be extremely thin and transparent to an electron beam. Shadow-like image is formed in varied darkness according to the density; the darker area represents the denser part of the sample while the lighter area represents the less dense part.

3.4.6 X-ray Photoelectron Spectroscopy (XPS)

XPS is necessary to analyze surface chemistry, composition and electronic state of the sample and to determine the degree of oxidation in GO and rGO. This technique was analyzed by using photoemission spectroscopy (PES) beamline, BL3.2a, of the Synchrotron Light Research Institute in Thailand. The PES system is equipped with a Thermo VG Scientific CLAM2 electron spectrometer and operated in the conditions of maximum photo energy 600 eV with an energy step of 0.1 eV. The data is analyzed using the Visual Basic macro based on the MS Excel program.

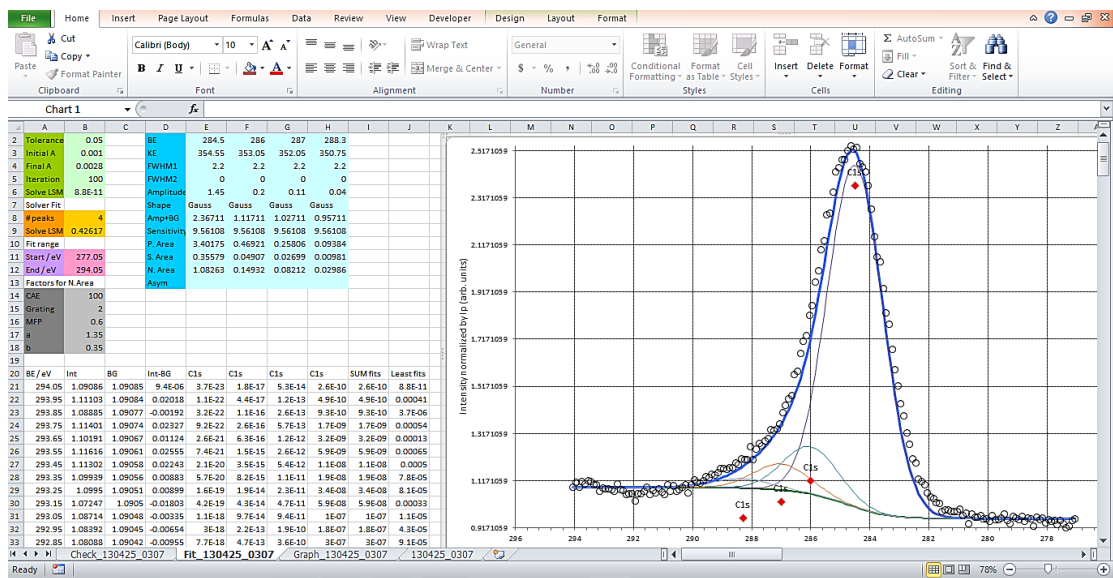


Figure 3.11 Screenshot of Visual Basic Macro software

CHAPTER 4 : RESULTS AND DISCUSSION

4.1 Introduction

The characterization results and applications made throughout this whole work duration are presented in this chapter. It begins with part I followed by part II, both consist of characterizations and application sections. In part I of the characterizations section, the crystal structure, optical properties and morphology of the commercial ZnO and P25 photocatalysts in powder and immobilized form are shown by XRD, UV-vis absorption and FESEM technique. As for part II, the crystal structure, optical properties and morphology of the synthesized samples are shown by XRD, UV-vis absorption, Raman, XPS, FESEM and HRTEM technique. These characterization analysis are carried out to study if the structure of the nanocomposite was affected by the presence of rGO. In part I of the application section, the comparison in performance between commercial ZnO and P25 during photocatalysis under UV and solar light, and CV experiment are presented. The results show that the ZnO was more efficient than P25 in degrading MB solution under solar light. In addition, it is found that slurry photocatalyst is better than immobilized photocatalyst, due to the high interfacial area between the powder photocatalyst and MB solution. While for part II, the application for synthesized samples on photocatalysis and photocurrent experiment are presented. ZnO/rGO nanocomposites showed enhanced performance in both photocatalysis and photocurrent experiments.

4.2 Part I

4.2.1 Characterizations of nanomaterials

4.2.1.1 XRD

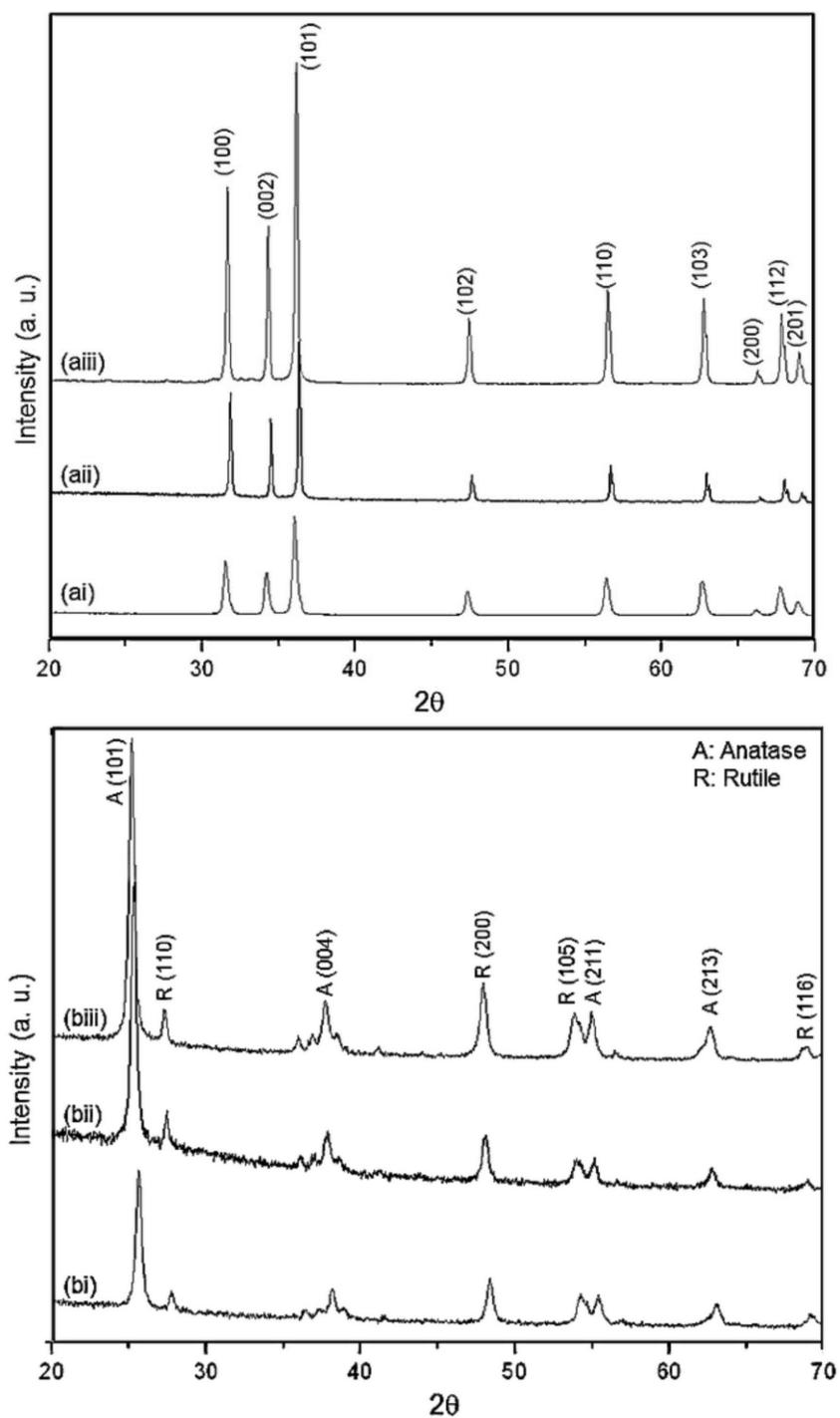


Figure 4.1 XRD patterns of (ai) calcined ZnO powder, (aii) calcined ZnO film, (aiii) ZnO pure powder (bi) calcined P25 powder, (bii) calcined P25 film, (biii) P25 pure powder

Figure 4.1 shows the XRD patterns of both ZnO and P25 before and after calcination, in the form of immobilized film and pure powder. As shown in the Figure 4.1 (ai), (aii), and (aiii), all diffraction peaks which correspond to the (100), (002), (101), (102), (110), (103), (200), (112), and (201) planes of ZnO and which can be indexed to the hexagonal wurtzite structure of ZnO (Kashyout, Soliman, Hassan, & Abousehly, 2010). Meanwhile in Figure 4.1 (bi), (bii), and (biii), all diffraction peaks correspond to the (101), (110), (004), (200), (105), (211), (213) and (116) planes of TiO₂ and it can be indexed to rutile and anatase phase of TiO₂ (Sakurai & Mizusawa, 2010). No other peaks detected for both ZnO and P25 which indicates the absence of any other impurities. The insignificance change in the XRD patterns clearly indicates that the ZnO and P25 retained their structures even when exposed to heat treatment or harsh condition.

4.2.1.2 UV-Vis spectral studies

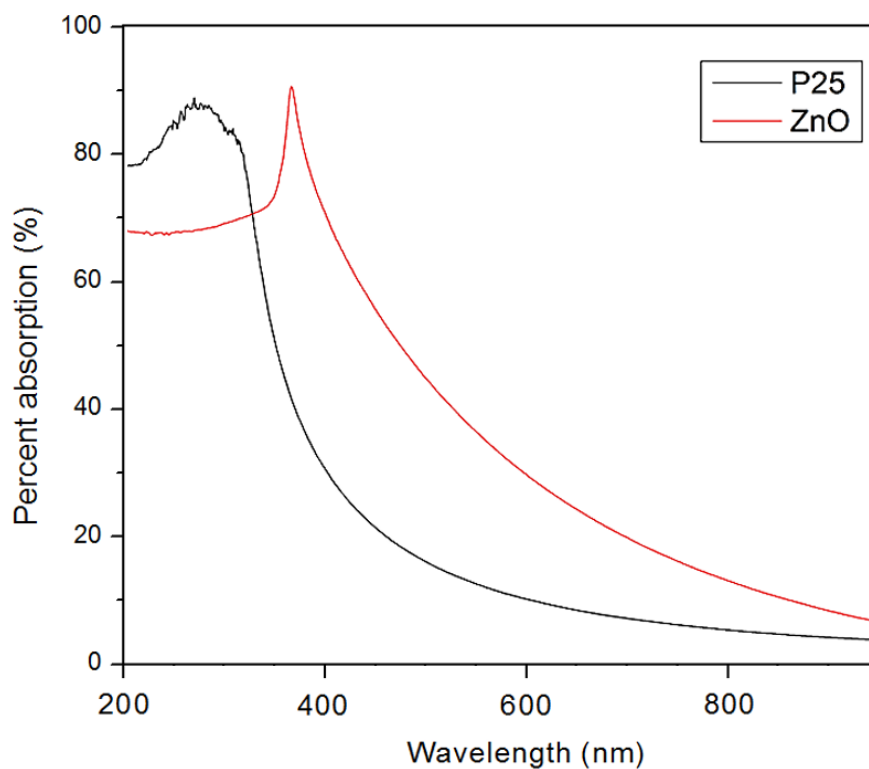


Figure 4.2 UV-Vis spectra of ZnO and P25

Figure 4.2 illustrates the absorption spectra of ZnO and P25. The spectra show that P25 absorbs mainly in the UV region and the absorption peak reached almost zero after 380 nm,

while the absorbance of ZnO is more compared to P25 mainly in the visible region within the range from 300 to 500 nm. High absorption of visible light by ZnO indicates that ZnO absorbs a large fraction of solar spectrum than P25 (Sakthivel et al., 2003).

4.2.1.3 FESEM

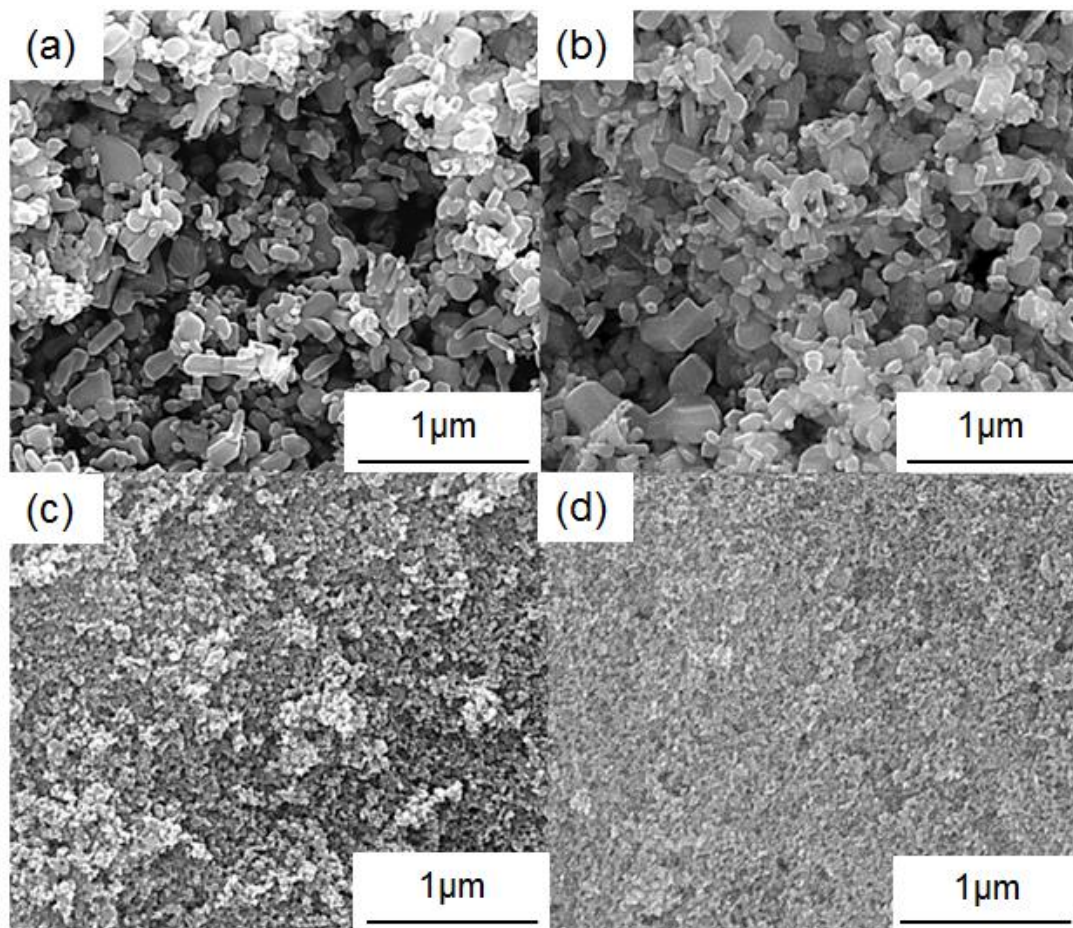


Figure 4.3 SEM images of (a) calcined ZnO powder, (b) calcined immobilized ZnO, (c) calcined P25 powder and (d) calcined immobilized P25

Figure 4.3 shows the SEM images of ZnO and P25 morphologies after calcination. Both ZnO and P25 exhibit the same morphologies either they were in powder or immobilized film form. The average sizes of ZnO and P25 are 100 nm and 30 nm, respectively.

4.2.2 Applications

4.2.2.1 Photocatalysis

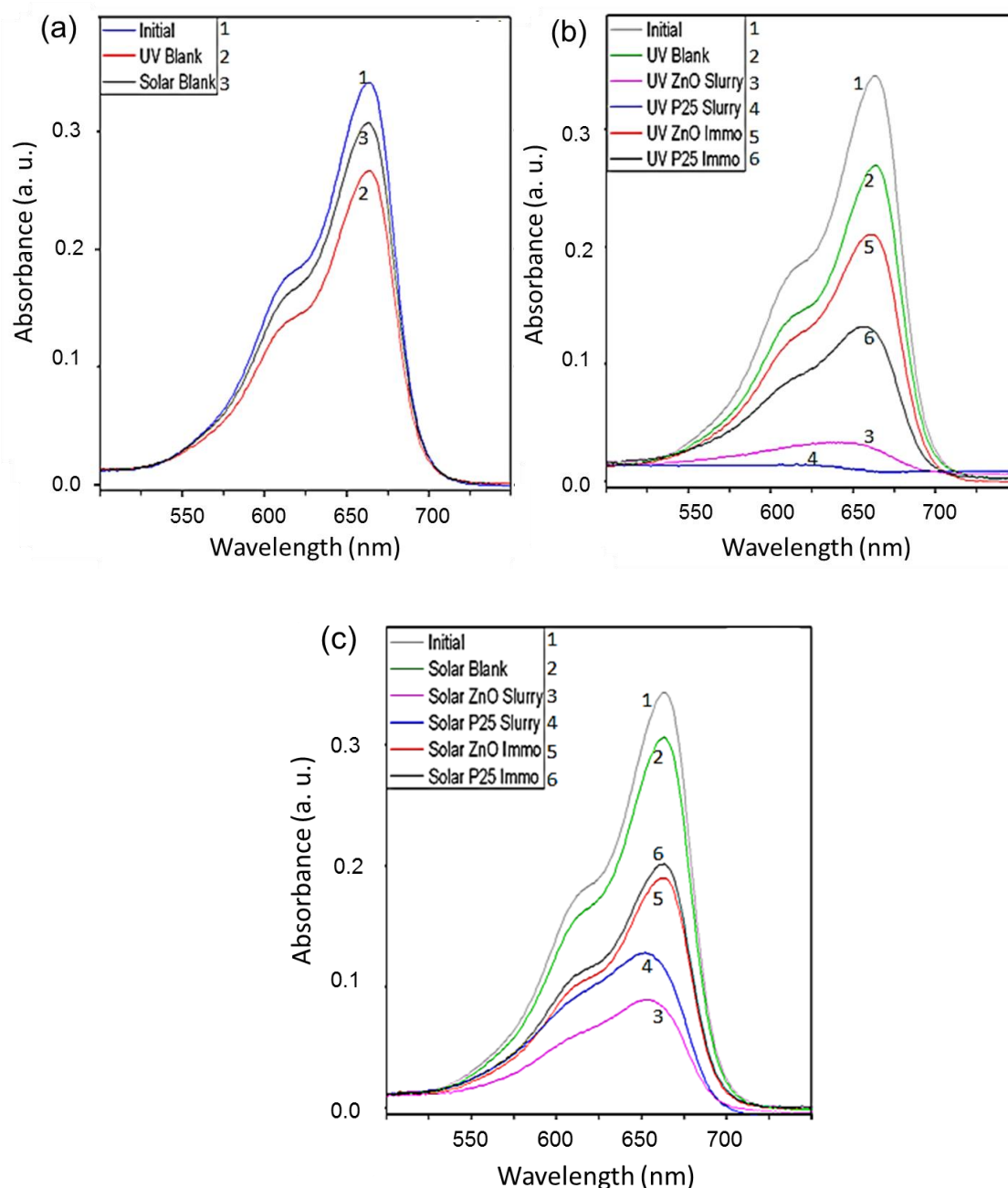


Figure 4.4 UV-Vis absorption spectra of the MB solution (a) without photocatalyst, (b) with photocatalyst under UV light, and (c) with photocatalyst under solar light illumination

Figure 4.4 illustrates the absorbance spectra of MB solution concentration with maximum peak at 663 nm. Figure 4.4 (a) shows comparison of MB concentration between initial concentration, after exposed under UV and solar light, respectively. The photocatalytic degradation of MB without photocatalyst under light exposure is due to photolytic reaction

induced through light absorption by MB molecules (Tschirch et al., 2008). The peak of MB under UV light exposure is lower than under solar light showing that the UV light photon has higher energy than solar light. Figure 4.4 (b) illustrates the absorption spectra of MB degradation under UV irradiation by both ZnO and P25 slurries and immobilized form. The photocatalytic degradation of MB in the presence of photocatalyst P25 is lower compared the ZnO, both in slurry as well as in the immobilized form. This shows that the photocatalytic activity of P25 is higher than ZnO due to high UV light absorption property of P25. Figure 4.4 (c) illustrates the temporal absorption spectral change of MB due to the photodegradation under solar irradiation by ZnO and P25, both in slurries and immobilized form. However, the results are contradicted with the degradation of MB under UV light as shown in Figure 4.4 (b). The photodegradation of MB in the presence of ZnO is lower when compared to the P25 both in slurry and immobilized form (Figure 4.4 (c)). This is mainly attributed to the absorption capability of wide range of solar light by ZnO, whereas the P25 can only absorb the 2-3 % of UV light of the solar spectrum (Saleh, 2011). Based on both Figure 4.4 (b) and Figure 4.4 (c), the photocatalytic degradation of MB by ZnO and P25 in slurry form is more efficient than that of the immobilized form. The better performance by slurry photocatalysts is due to the high amount of surface active sites when the photocatalyst in suspension.

4.2.2.2 Cyclic voltammetry (CV)

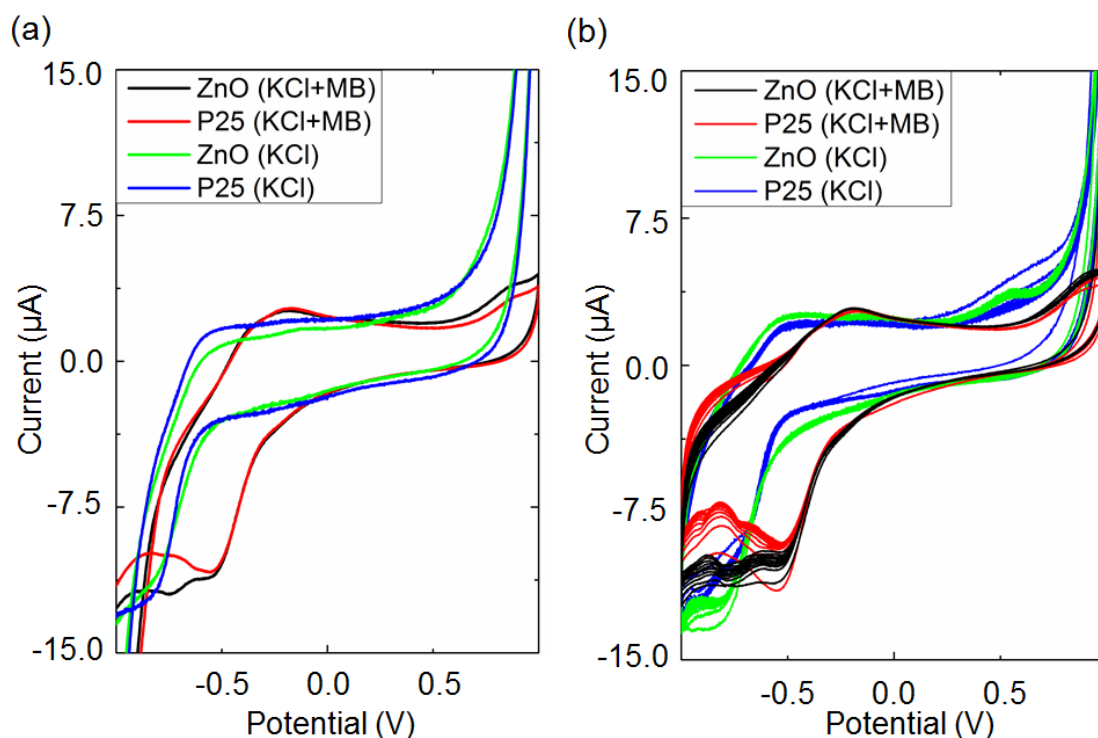


Figure 4.5 a) CV and (b) multiple CV of modified GCE in 0.1 M of KCl solution with and without the presence of 1.5 ppm of MB

Figure 4.5 (a) exhibits the CV of ZnO and P25 photocatalysts modified GCE with in KCl as a supporting electrolyte. It can be seen there is no oxidation or reduction peak observed. When the MB is spiked into the KCl solution, on the forward scan, an oxidation peak appeared at -0.25 V, upon scan reverse a reduction peak appeared at -0.5 V. Multiple sweeps as shown in Figure 4.5 (b), it shows after ten potential cycles, the oxidation and reduction peaks only shifted slightly. This shows that the presence of MB not influence much on the oxidation and reduction process as the peaks are almost at the same amplitude. This suggest that the coated photocatalysts on the GCE surface was stable and no leaching photocatalyst occurred from the electrode surface (Pakapongpan et al., 2011).

Figure 4.6 shows the CV pattern obtained from bare and modified GCE in the dark for 2 h. It can be observed [Figure 4.6 (a), (b) and (c)] that the intensity of the redox peaks remained

the same, indicating the degradation of MB did not happen in the absence of light and it indicates the photocatalyst only active upon irradiation.

However, the CV patterns changed when illuminated with solar light as shown in Figure 4.7. When bare GCE is used [Figure 4.7 (a)], there is no significant change in cycles after 2 h, indicating redox process of MB solution is hardly happened in the absence of photocatalyst. On the contrary, when GCE is modified with the photocatalyst, the decrement and increment of the cycles can be seen as shown in Figure 4.7 (b) and Figure 4.7 (c). This indicates the significant electrochemical reaction between photocatalyst and MB molecules occurred upon the solar light illumination. Notice that the CV pattern by ZnO and P25 shows different direction in shift of peak which can be related with the absorptive behavior of the MB (Mandal & Bhattacharyya, 2012). Based on Figure 4.7 (b), the oxidation peak increased and the reduction peak decreased with increasing time of solar light illumination. This shows that the MB solution is gradually oxidized by the ZnO. While based on Figure 4.7 (c), both the oxidation and reduction peak are increased with increasing time of solar light illumination, shows that the MB was adsorbed on P25 surface. From the different CV patterns shown, suggesting that the MB solution were directly degraded by ZnO, while for P25, the adsorption takes place during photocatalysis. This analysis proved that ZnO and P25 have different mechanism of photodegradation.

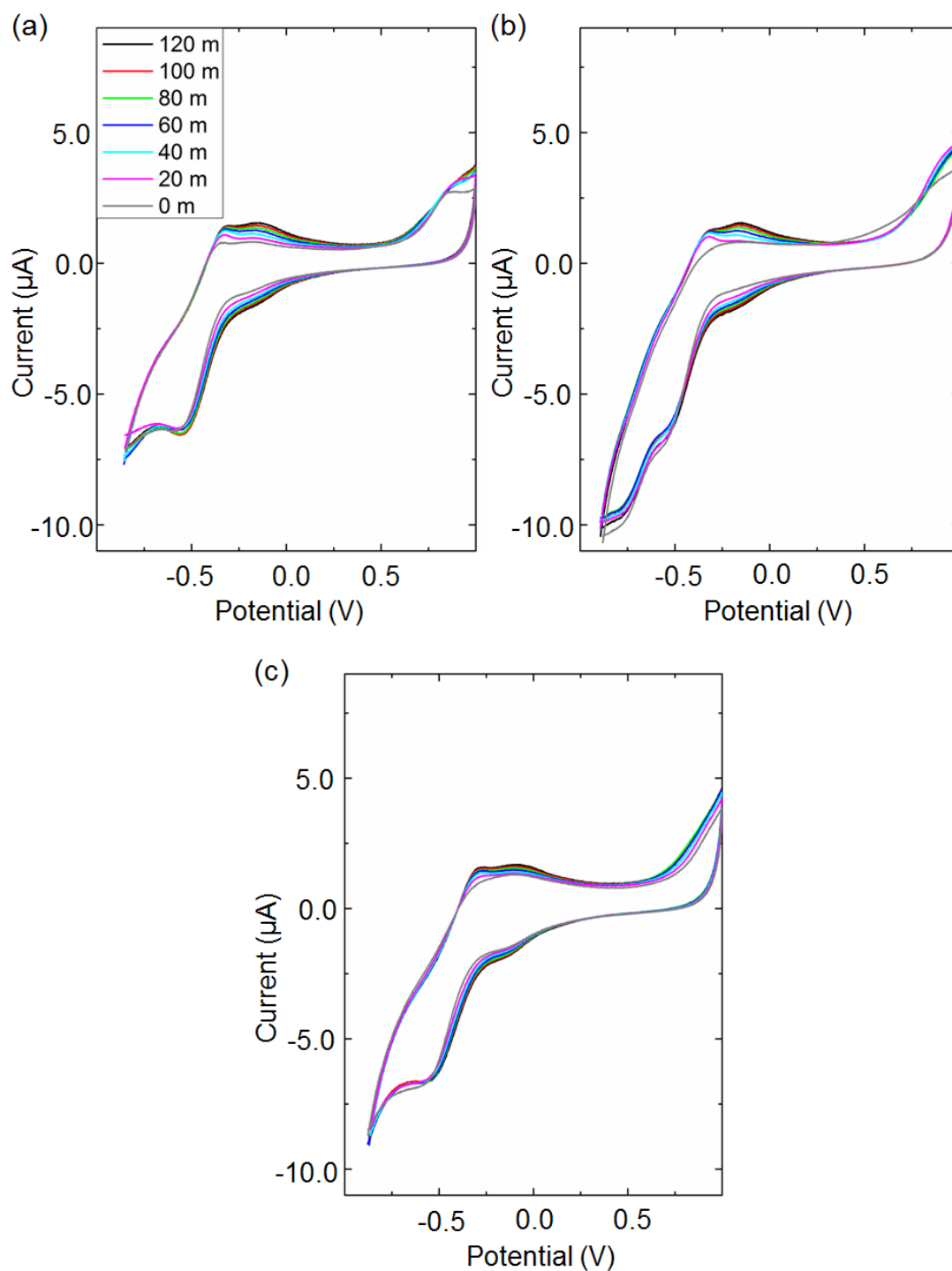


Figure 4.6 CV for (a) bare GCE, (b) ZnO-modified GCE, and (c) P25-modified GCE in 0.1 M of KCl solution spiked with 1.5 ppm of MB left in the dark for 2 hours (m: minutes)

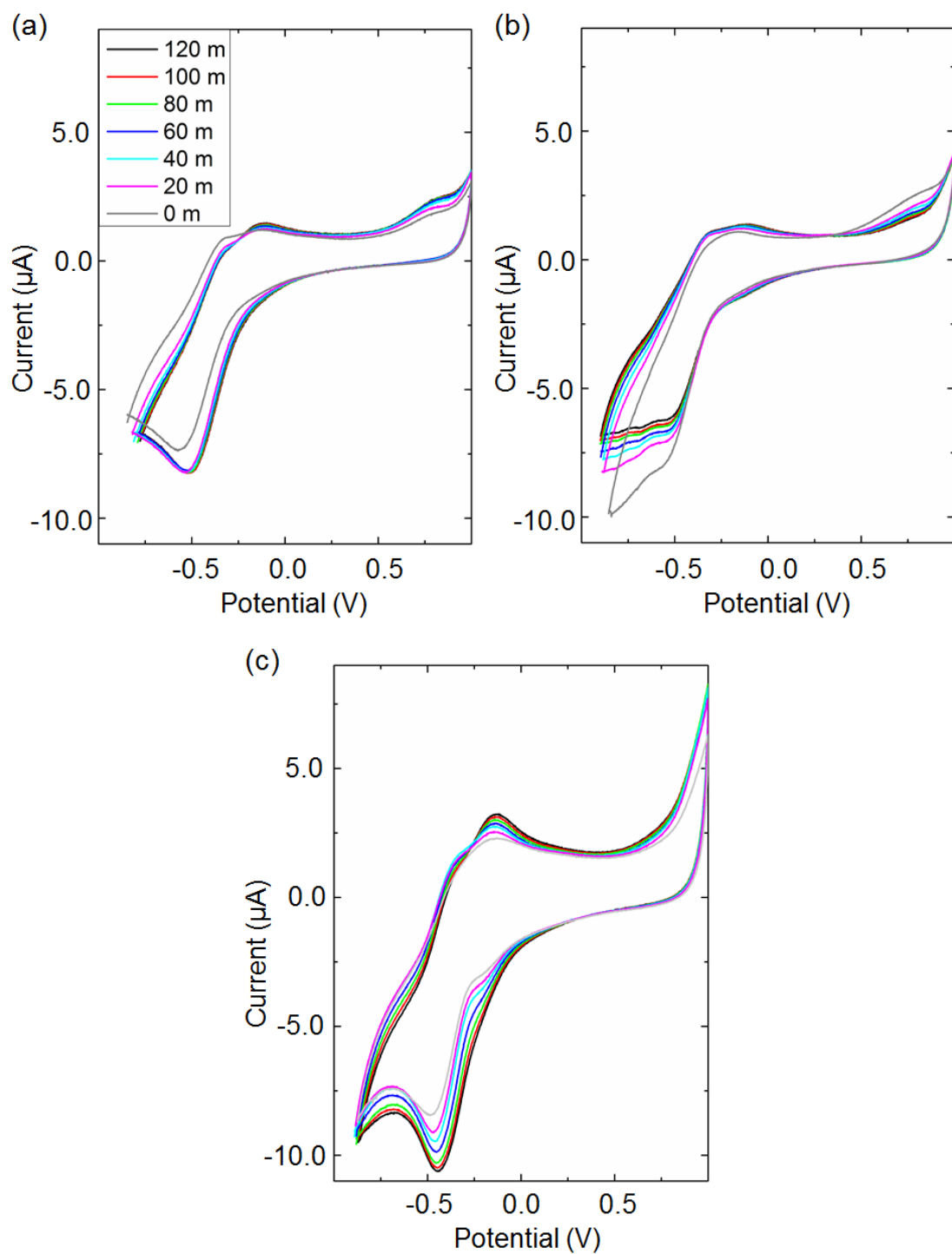


Figure 4.7 CV for (a) bare GCE, (b) ZnO-modified GCE, and (c) P25-modified GCE in 0.1 M of KCl solution spiked with 1.5 ppm of MB illuminated with solar light for 2 hours (m: minutes)

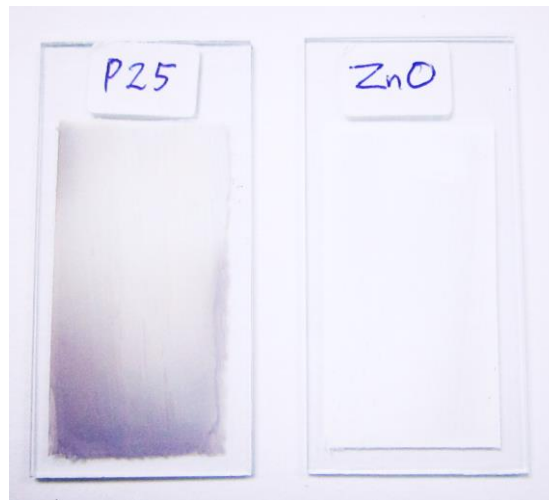


Figure 4.8 Immobilized P25 and ZnO film after the photocatalysis process

Figure 4.8 shows the condition of both immobilized ZnO and P25 after photocatalysis experiment. It can be seen that there is tainted blue colour on the surface of the immobilized P25, whereas, the surface of immobilized ZnO remained white due to different mechanism of photodegradation by ZnO and P25 as explained in Figure 4.7.

4.3 Part II

4.3.1 Characterization of nanocomposites

4.3.1.1 XRD

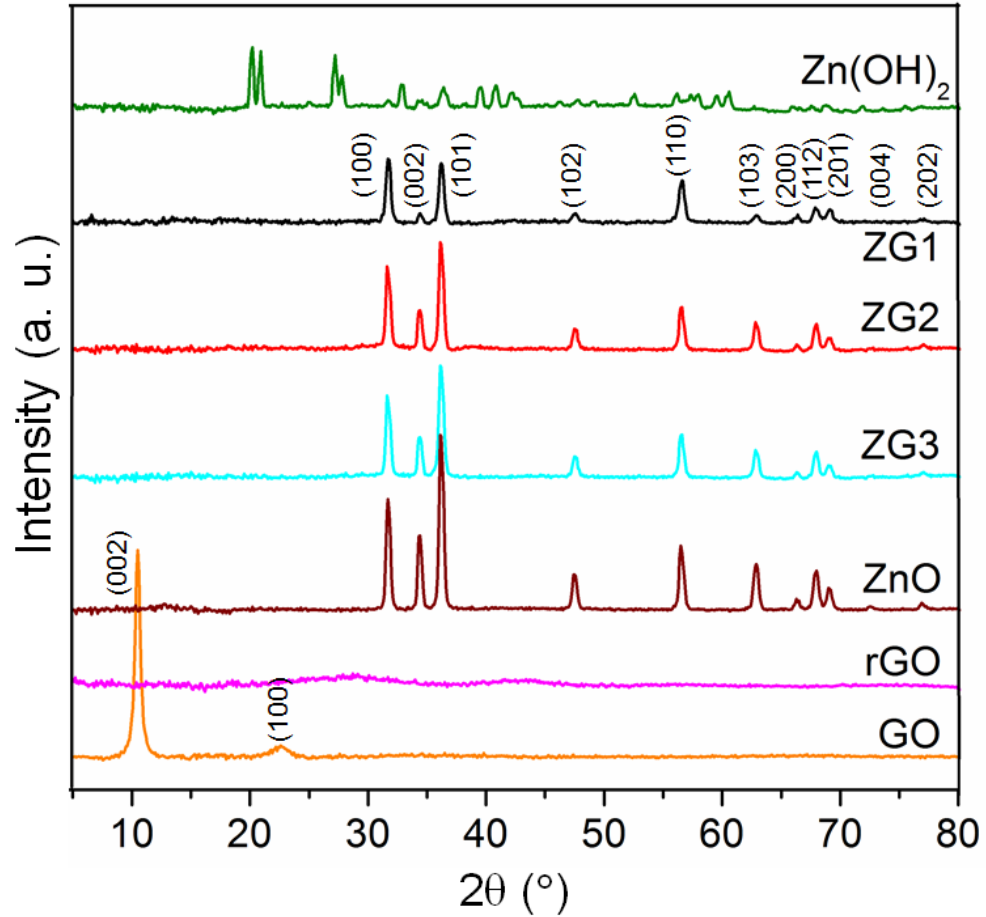


Figure 4.9 XRD patterns of GO, rGO, ZnO, ZG1, ZG2 and ZG3

XRD patterns were recorded for ZnO before microwave treatment namely (Zn(OH)_2), ZnO, nanocomposites and rGO synthesized by microwave method, and GO are shown in Figure 4.9. XRD pattern of GO shows one prominent peak located at 11.1° corresponds to the (002) plane of GO. This peak can be ascribed to the attachment of oxygenated functional groups on the GO sheets (Y. Li, Gao, Ci, Wang, & Ajayan, 2010). While for rGO, it shows two small bumps appeared at 2θ value of 29° and 44° , which indicates the oxygen functional groups are removed and replaced with the formation of disordered graphene sheets (Singh et

al., 2012). There are eleven diffraction peaks can be observed for ZnO at the 2θ value of 31.8° , 34.6° , 36.2° , 47.6° , 47.7° , 56.6° , 63.1° , 66.6° , 68.1° , 69.3° , and 77.2° , which correspond to (100), (002), (101), (102), (110), (103), (200), (112), (201), (004), (202), (104), and (203) planes, respectively. All the peaks can be indexed to hexagonal phase wurtzite structure of ZnO (JSPDS No. 80-0074). The peaks also can be seen at the ZG1, ZG2 and ZG3, which are similar to those of ZnO, indicating the ZnO nanorods on the rGO sheets have the same structure as ZnO. This also shows that the structure of ZnO particles is not influenced by the presence of rGO. The disappearance of the GO peak suggests the complete exfoliation of GO due to the insertion of ZnO particles (Vijay Kumar, Huang, Yusoff, & Lim, 2013). For Zn(OH)_2 , it shows several peaks which can be indexed to orthorhombic phase of Zn(OH)_2 . The different patterns showed by Zn(OH)_2 , ZnO and nanocomposites indicating that the microwave treatment is a promising method for the synthesis of ZnO structure. No diffraction peaks detected from impurities.

4.3.1.2 UV-vis absorption spectral studies

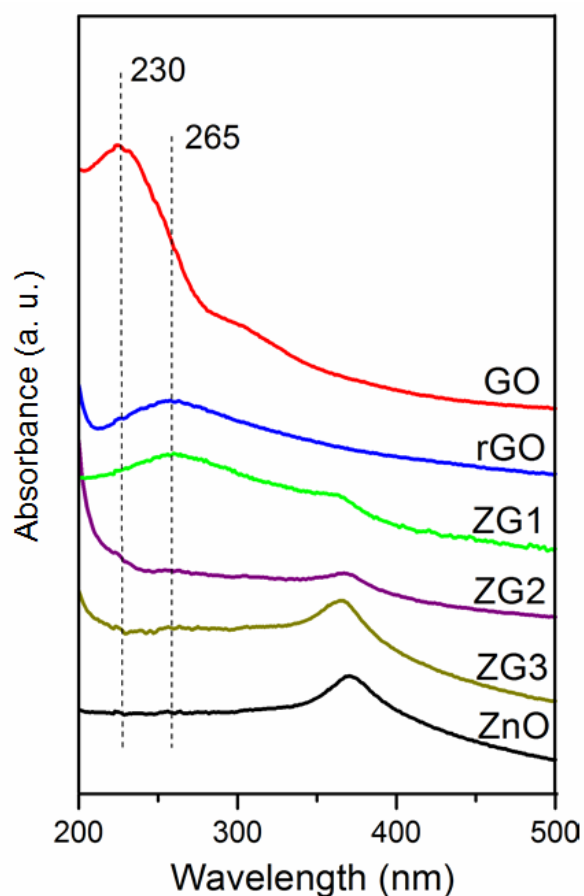


Figure 4.10 UV-Vis spectra of GO, rGO, ZnO, ZG1, ZG2 and ZG3

Figure 4.10 shows the UV-Vis absorption spectra of ZnO, nanocomposites, GO and rGO. The ZnO exhibit a typical absorption peak at 360 nm which can be assigned to the intrinsic band-gap absorption of ZnO. While the nanocomposites show the red-shift of the ZnO absorption edge corresponding to the ZnO which is attributed to the chemical interaction between ZnO and rGO (Yang & Liu, 2011). In addition, comparing ZG1, ZG2 and ZG3, the relative amplitude of the carbon peak (~265 nm) increases with increase the rGO loading. The GO shows a maximum absorption peak at 230 nm, indicating to the $\pi \rightarrow \pi$ transition of the aromatic C-C bonds. After the reduction of GO, the absorption peak at 230 nm red-shifted to 265 nm, indicating that the π conjugation was revived within the rGO sheets (Kim & Min, 2012).

4.3.1.3 Raman spectra

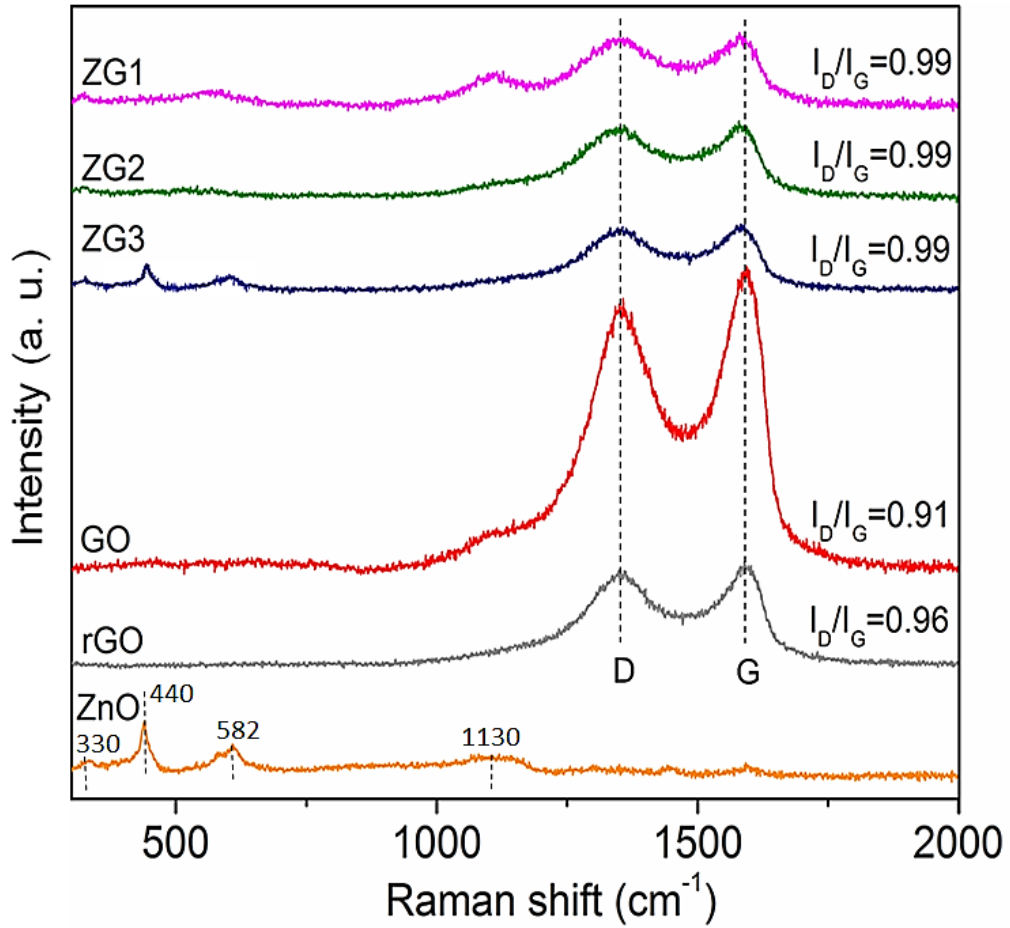


Figure 4.11 Raman spectra of GO, rGO, ZnO, ZG1, ZG2 and ZG3

In Fig. 4.11, the spectrum for ZnO displays a peak at 330 cm^{-1} which is assigned to the second-order Raman spectrum, originating from the zone-boundary phonons of hexagonal ZnO. The main dominant sharp peak at 440 cm^{-1} can be labeled to E2 (HI) mode, demonstrating the characteristic peak of the hexagonal wurtzite phase ZnO. The peak at 582 cm^{-1} is assigned to E1 (LO) mode, attributed to the formation of oxygen deficiency, or other defect states in ZnO. The peak at 1130 cm^{-1} is due to the multiple-phonon scattering processes (J. Y. Li, 2008). Lower peak intensity is observed in composites as compared to that in ZnO indicating the interaction occur between ZnO and rGO.

Raman also can be used to investigate the properties and disorder of graphene by observing the intensity of prominent bands known as G band and D band. G band refers to the

presence of sp^2 carbon type structure which is often used to measure the quality of graphene, while D band refers to the presence of some disorder in the graphene structure. Increase in intensity ratio of D/G value indicates a high degree of disorder. From the Figure 4.6, the I_D/I_G value of rGO (0.96) was larger as compared to the GO (0.91) due to the decrease in average size of sp^2 domain effects from the reduction process. This means that the graphitic structure is broken into smaller fragments resulted a lot of edges. These edges actually are the defects that cause the increase of I_D . The I_D/I_G value of nanocomposites was larger (0.99) as compared to the value of GO (0.91) and rGO (0.96). This is due to the increasing disorder of sp^2 conjugation, effects from the presence of ZnO particles in the nanocomposites (Stankovich et al., 2007).

4.3.1.4 XPS

XRS measurement was performed to study about the samples composition, the kind of oxygen species present and level of oxidation.

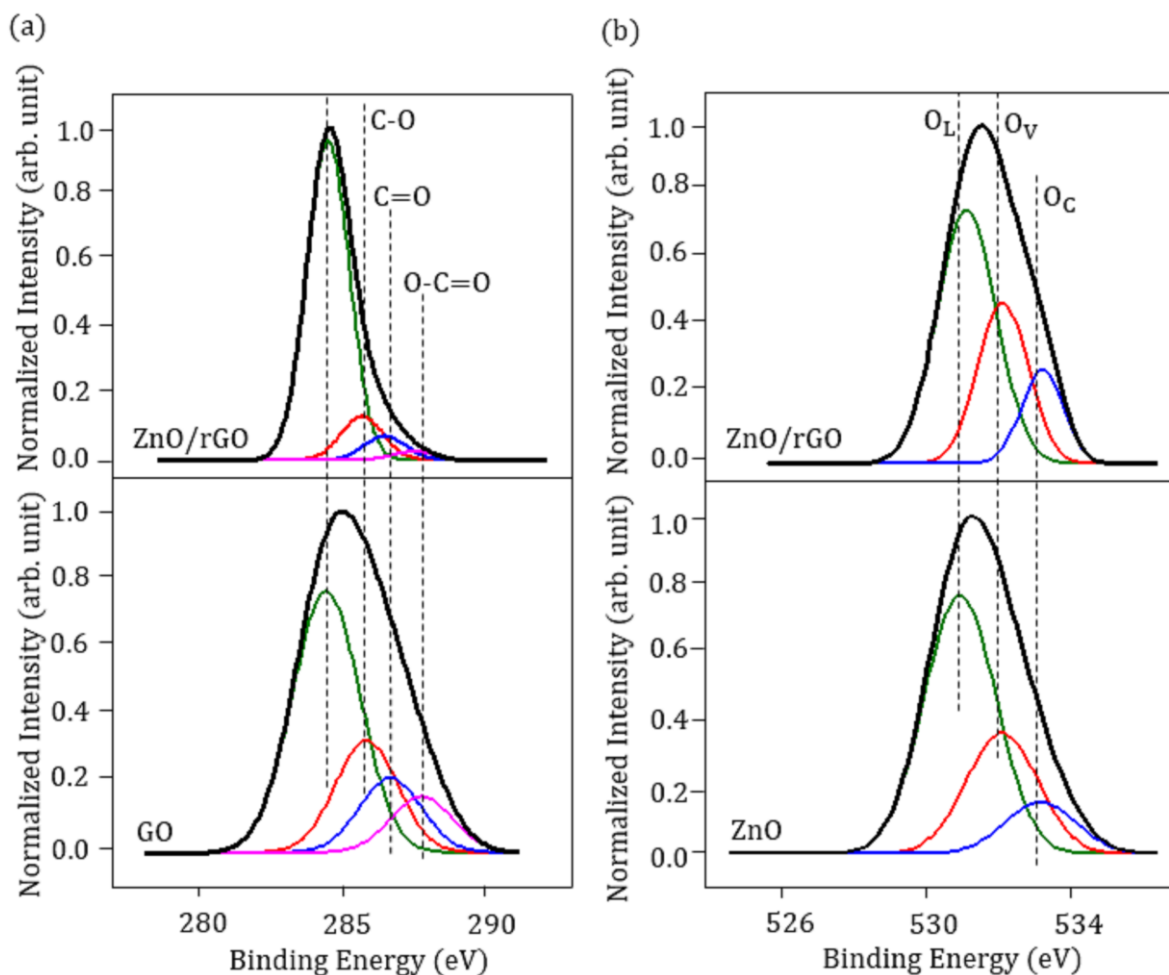


Figure 4.12 XPS spectra of (a) C1s of GO and ZG1, (b) O1s of ZnO and ZG1

The electrical bonding between rGO and ZnO is analyzed by XPS. Figure 4.12 (a) illustrates the comparison of carbon region between GO and the composite. This region can be deconvoluted into four Gaussian peaks corresponding to non-oxygenated carbon and oxygen-bonded carbon, namely sp^2 carbon (C-C, 284.5 eV), carbon in C-O bonds (286 eV), carbonyl carbon C=O (287.4 eV) and carboxylate carbon O-C=O (288.8 eV) group. It can be

seen that the oxygenated-bonded carbon peaks still remained in the nanocomposite with the fact that these groups are hard to remove even after any reduction treatment. Nevertheless, there is an obvious different in their peak intensity, where the nanocomposites peak is much lower as compared to that of GO. This shows that the GO in the nanocomposite is reduced after the microwave treatment (Hofsäss et al., 2013).

Meanwhile, the oxygen region of ZnO and the nanocomposite are shown in Figure 4.12 (b). This region can be deconvoluted into three Gaussian peaks. The first peak at 529.8 eV is attributed to O^{2-} ion in the Zn-O bonds, labeled as O_L (oxygen lattice). The second peak at 531 eV is assigned to oxygen deficient defect, labeled as O_V (oxygen vacancy), and the last peak at 532.1 eV which is belonging to the presence of loosely bound oxygen; adsorbed O_2 and H_2O on the ZnO surface, labeled as O_C (chemisorbed oxygen species). Notice that for the nanocomposite, there is increased in binding energies with the peaks positioned at 530, 531.2 and 532.3 eV. Furthermore, it can be observed that the O_V peak of the nanocomposite has significant higher intensity compared to ZnO, revealing the density of oxygen vacancies on the ZnO surface is increased. The oxygen vacancies act as electron trap, leading to higher optical absorption and increasing the duration of the separated electrons and holes to form more hydroxyl radicals (Prakash et al., 2013).

4.3.1.5 FESEM

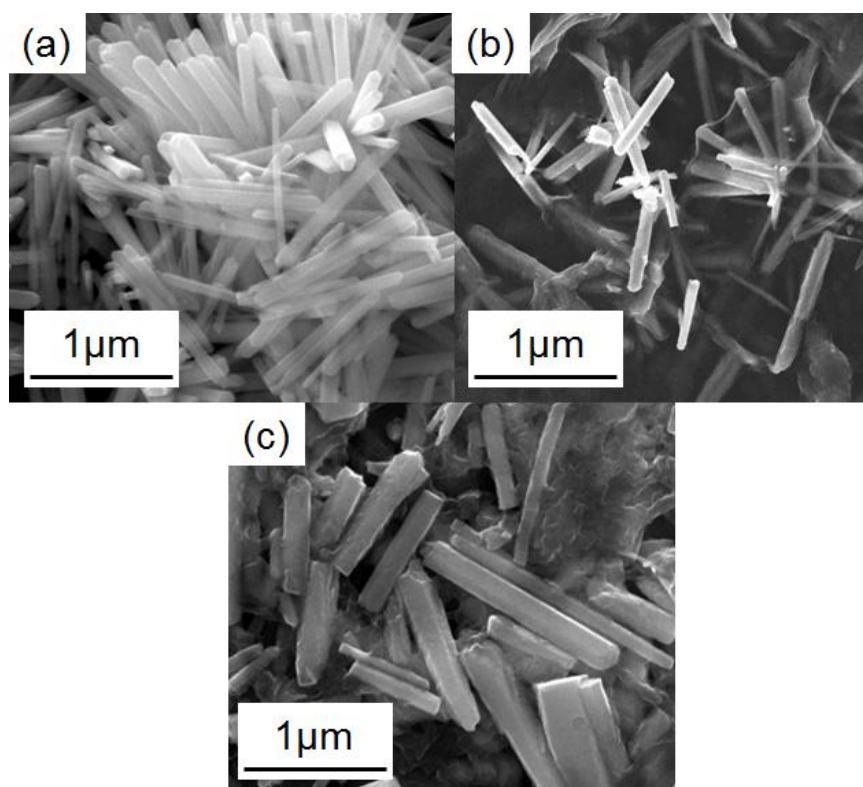


Figure 4.13 FESEM images of (a) ZnO, (b) ZG1 and (c) ZG

The FESEM images were recorded for the nanocomposite in the absence and presence of DETA for comparison and are shown in Figure 4.13. The nanocomposite in the absence of DETA shows the non-uniform and larger size of ZnO nanorod as compared to the nanocomposite with the presence of DETA [Figure 4.13 (b)]. This is due to the interaction between Zn^{2+} with DETA that formed Zn-DETA complex. The Zn-DETA complex hindered the fast reaction of Zn^{2+} with OH^- , forming ZnO nanorods with smaller diameter (Yi et al., 2008).

4.3.1.6 EDX

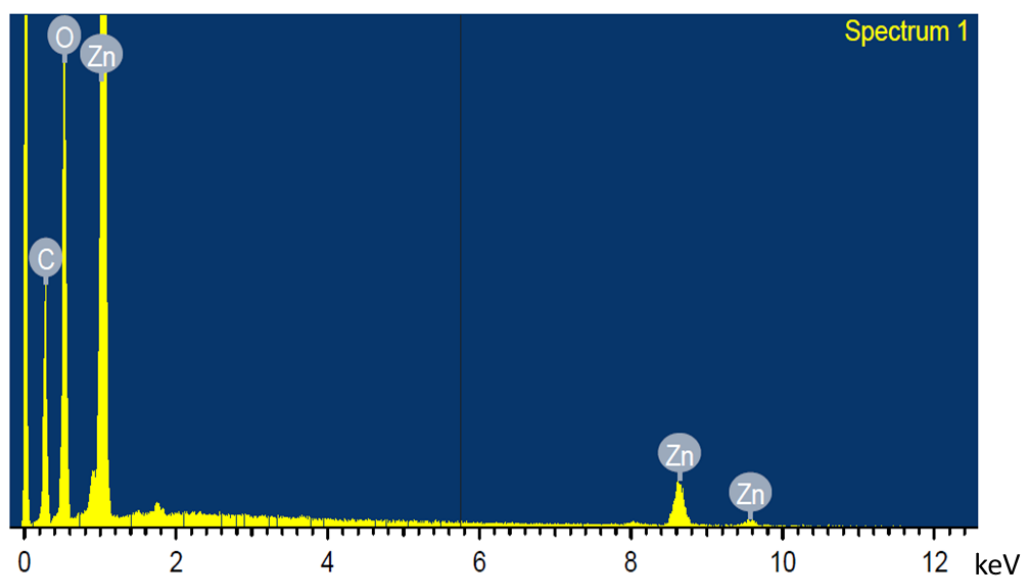


Figure 4.14 EDX spectrum of ZG1 nanocomposite

Figure 4.14 illustrated the corresponding EDX spectrum of ZG1 nanocomposite. The spectrum revealed the presence of C in addition to Zn and O. These signals indicate successful attachment of ZnO on the rGO surface. No other signal from other element is observed confirmed that the sample is ZnO/rGO nanocomposite.

4.3.1.7 HRTEM

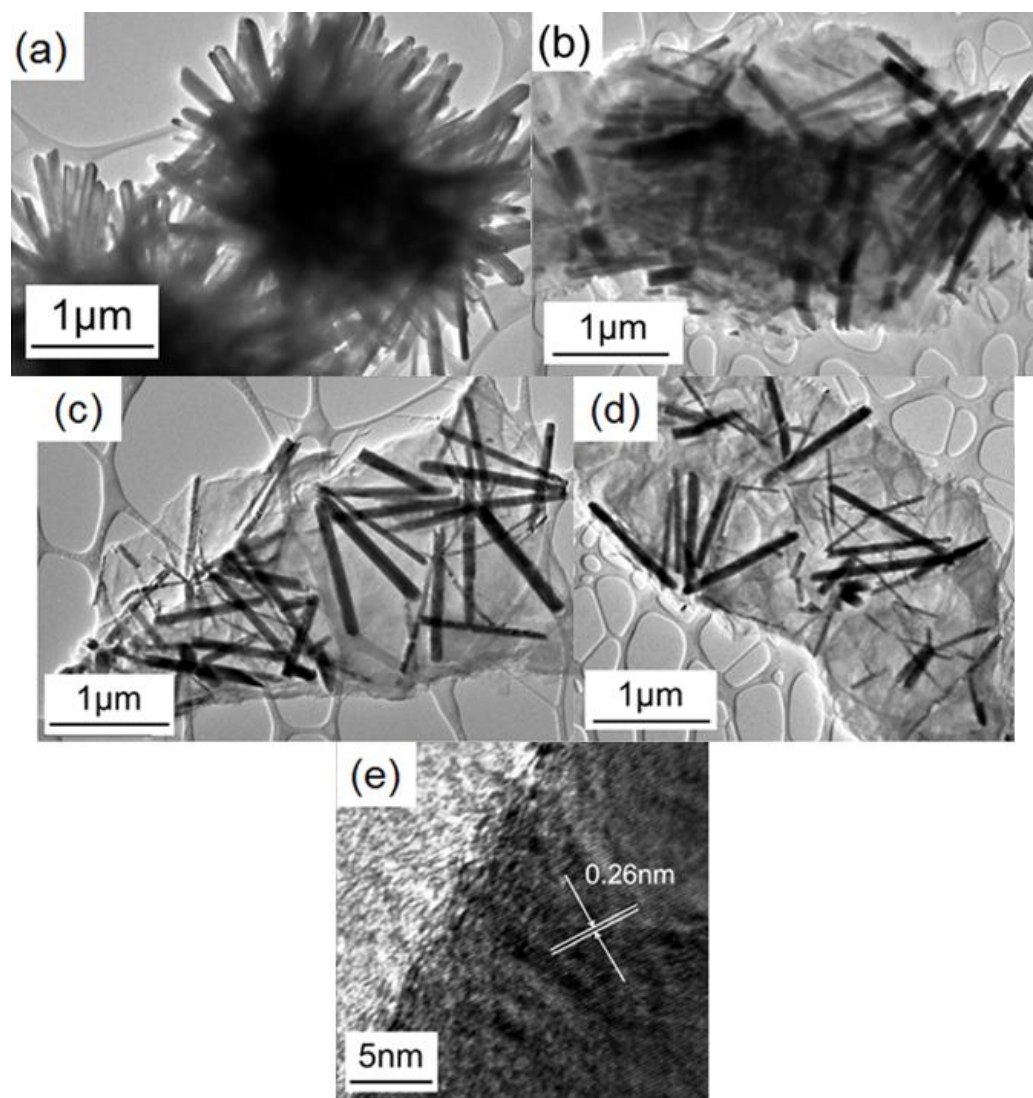


Figure 4.15 HRTEM images of (a) ZnO, (b) ZG3, (c) ZG2, (d) ZG1 and (e) ZG1 at a higher magnification

Figure 4.15 (a) revealed the ZnO nanorods apparently originated from the centre, forming flower-like morphologies. Meanwhile, the ZnO rods are distributed on the surface of rGO for all the nanocomposites, confirming the interaction between ZnO and rGO. The average diameter of the ZnO nanorods in the nanocomposite (Figure 4.15 (b), (c) and (d)) are slightly decreased with increasing of rGO content due to the higher number of reaction sites provided by the GO that inhibited the agglomeration of ZnO particles (Tan et al., 2013). The smaller size of the ZnO in the nanocomposites provides the larger effective surface area in the enhancement of dye adsorption and photocatalytic efficiency. The crystal lattice fringes

(Figure 4.15 (e)) with a d-spacing of 0.26 nm can be assigned to the (002) plane of hexagonal ZnO (Ye et al., 2009).

4.3.2 Applications

4.3.2.1 Adsorption and photocatalysis

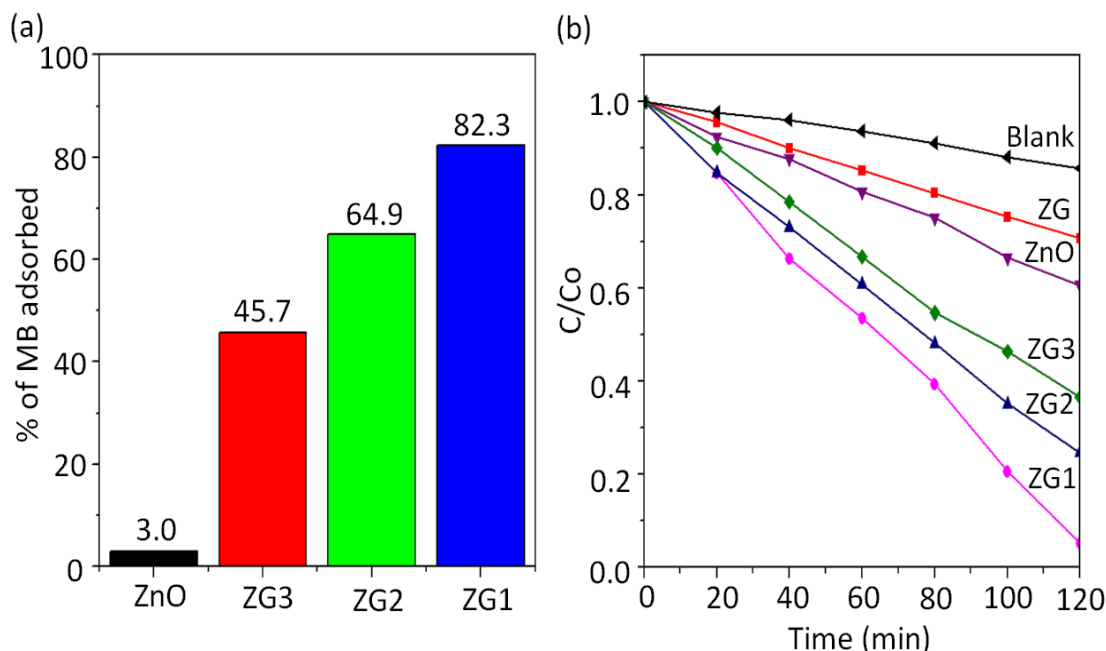


Figure 4.16 (a) Adsorption performance of ZnO, ZG1, ZG2 and ZG3 in the dark. (b) Photodegradation performance of blank (without photocatalyst), ZnO, ZG, ZG1, ZG2 and ZG3 under the sunlight

Figure 4.16 (a) displayed the percentage of MB solution adsorbed by the sample after 18 hours stirring in the dark. As can be seen in the figure, the ZnO showed 3% of MB adsorption. Meanwhile for nanocomposites, the adsorption rate increased to 45.7%, 64.9% and 82.3% for ZG3, ZG2, and ZG1, respectively. The MB adsorption efficiency increased with increasing the rGO proportion in the nanocomposites. This is attributed to the π - π stacking interactions are involved between the aromatic MB molecules and the aromatic rGO (Liang et al., 2010). Figure 4.16 (b) showed the time-dependent degradation curves of MB solution by the same samples. Herein, the lower C/Co value defines the higher photodegradation of MB solution. As can be seen in the figure, MB exhibited low self-degradation whereas in the presence of photocatalysts especially for the nanocomposites, the MB is almost completely

degraded within 2 hours. The degradation rate for blank (without photocatalyst), ZG, ZnO, ZG3, ZG2, and ZG1 are 12%, 25%, 39.4%, 63.5%, 75.4% and 94.8%, respectively. The observed enhanced photocatalytic activity by the nanocomposites is largely attributed to the smaller diameter of the ZnO nanorod providing larger effective surface area that improves the adsorbance of MB, and the amount of rGO present that acts as a photosensitizer. rGO is photoexcited by sunlight and transferred electrons to the CB of ZnO, raising the concentration of electrons leading to dye degradation (Chen & Wang, 2014).

4.3.2.2 Cycle test

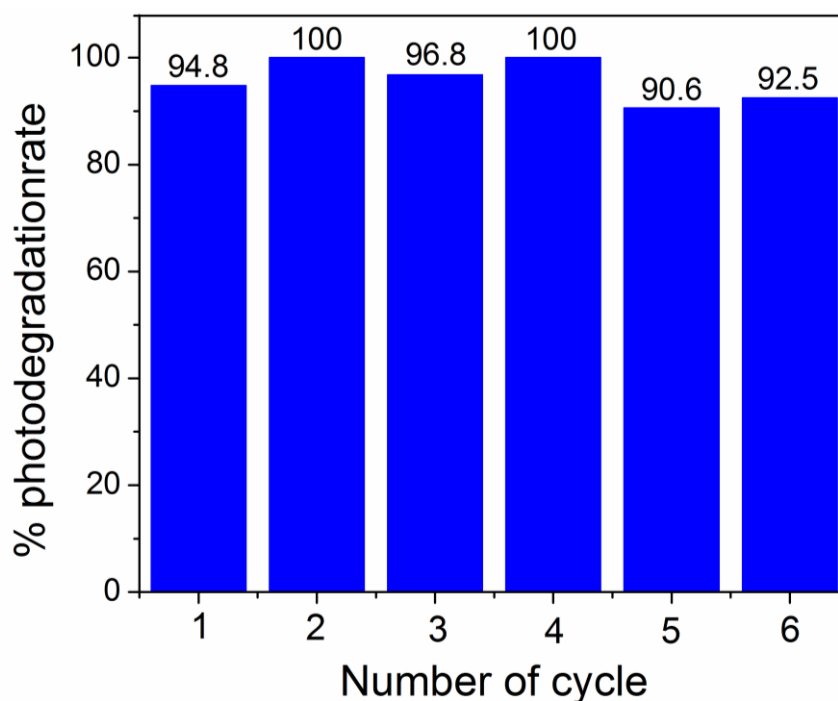


Figure 4.17 Cycling runs in the photodegradation of MB by ZG1 under the sunlight

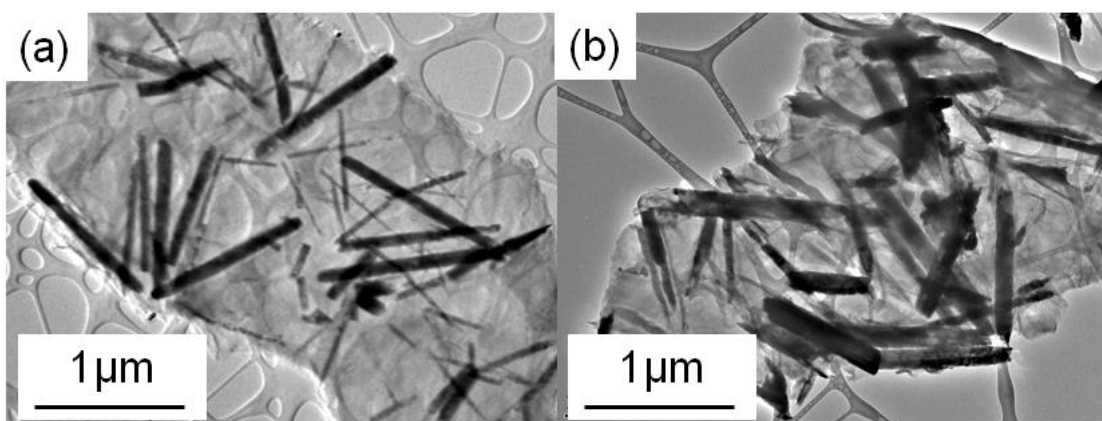


Figure 4.18 HRTEM image of (a) ZG1 before photocatalysis (b) ZG1 after six cycles

The lifetime and stability of photocatalyst during photocatalysis is a crucial factor for practical application which has a relationship with the working life. The reuse capability of ZG1 in photodegradation of MB is tested by repeating the photocatalytic experiment for six cycle using the same sample after the completion of the photocatalytic experiment shown in Figure 4.16 (a). As can be seen in Figure 4.17, the MB solution was almost completely absorbed and degraded by ZG1 for every cycle. From cycle 1 to cycle 6, the range of MB degradation is less than 10%, showing the rate of degradation is significant after six times of ZG1 reuse. ZG1 did not exhibit great changes in morphology even after the sixth cycle, showing that ZG1 is photostable (Figure 4.18). This study revealed that ZG1 demonstrated good stability and can be reuse.

4.3.2.3 Photocurrent

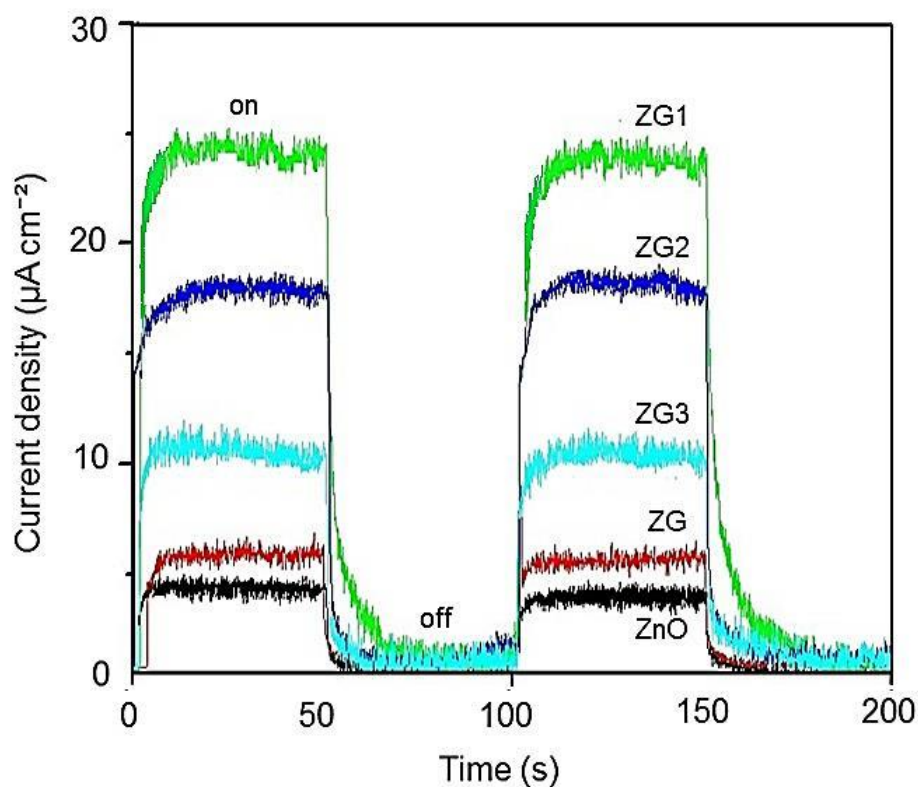


Figure 4.19 Photocurrent of ZnO, ZG, ZG1, ZG2 and ZG3 under solar light irradiation ([KCl] = 1 M)

Photoelectrochemical experiment was measured to investigate the mobility of photoinduced electron within the samples when the solar source was switched on and off. When the solar light was on at bias potential of 0.5 V, a uniform photoresponses were displayed in all electrodes. All the nanocomposite electrodes especially ZG1, ZG2 and ZG3 showed a much higher photocurrent density than the ZnO electrode where the photocurrent of ZG1 is about six times higher than that of ZnO. The photocurrents are $4.0 \mu\text{A cm}^{-2}$, $6.0 \mu\text{A cm}^{-2}$, $10.0 \mu\text{A cm}^{-2}$, $17.0 \mu\text{A cm}^{-2}$ and $24.7 \mu\text{A cm}^{-2}$ for ZnO, ZG, ZG3, ZG2 and ZG1, respectively. The generated photocurrent increased with the increase concentration of rGO in the nanocomposites, attributed to the synergistic effect between the ZnO nanorods and rGO within the nanocomposites under illumination (Durantini et al., 2012). These results are in agreement with the photocatalysis results (Fig. 4.16 (b)).

CHAPTER 5 : CONCLUSION AND FUTURE WORKS

5.1 Conclusion

From the results obtained, all of the research objectives have been achieved successfully. Under solar and UV irradiations, the photocatalytic activity shown by suspension ZnO and P25 photocatalysts were high as compared to immobilized counterpart due to the large interfacial surface which are possessed by suspension photocatalysts. Commercial ZnO and P25 reveal excellent performance in degradation of MB under UV light and solar light in the photocatalysis experiment. In addition, ZnO performed better than P25 under solar light radiation which suggested that ZnO can be an effective alternative material to P25. From these observations, it is suggested that ZnO and P25 have different photodegradation mechanism. In order to ascertain these observations, the investigation was proceeded by CV analysis. The analysis exhibited shifting of ZnO reduction peaks in different direction as compared with the reduction peaks shown by P25, which suggested that ZnO had mineralize MB immediately while P25 undergoes absorption before the degradation of MB. This analysis is strongly supported by the tainted blue color observed on the surface of P25 film while the ZnO surface still remained white.

Following this on the synthesis section, the whole process was carried out using a low temperature range technique. ZnO nanorods, with an average length:diameter ratio of 10, decorated rGO with high uniformity were successfully synthesized via a facile microwave method, using DETA as the capping agent. DETA acts as morphology controller where it allowed the formation of ZnO on rGO sheets with high uniformity and reduced the ZnO particles size. The formation of uniform ZnO and ZnO/rGO nanocomposite takes place within 30 min heating, proposing that the microwave method is a recommended method for synthesis. The structure, morphology and optical properties of the samples were characterized by XRD, UV-vis spectroscopy, Raman, FESEM, HRTEM and XPS techniques.

XRD results showed that the diffraction peaks of ZnO/rGO nanocomposite were similar to those of ZnO, which represents that the hexagonal wurtzite structure of ZnO did not change after the addition of rGO. UV-vis spectroscopy displays the red-shifting of ZnO absorption edge of ZnO/rGO nanocomposites with respect to that of ZnO, suggesting that the chemical interaction between ZnO and rGO has occurred. The formation of rGO also could be confirmed by observing the red-shifting of the rGO peak from 230 nm to 265 nm, indicating restoration of π conjugation within rGO sheets. The similar D and G peak of rGO were observed in ZnO/rGO nanocomposites, indicates that rGO structure is maintained in the nanocomposites. The intensity of D to G peaks ratio is analyzed and ZnO/rGO nanocomposites exhibit the highest value compared to GO and rGO, due to the increase of disordered sp^2 domains contribution from the presence of ZnO. The reduction of the GO is also confirmed through XPS analysis with the decrement of the oxygen-bonded carbon peaks intensity. The defects of ZnO were also studied and were discovered that ZnO/rGO nanocomposite exhibits higher intensity of the oxygen vacancy peak compared to ZnO. This suggests that the nanocomposite could improve the performance by trapping photo-excited electrons during photocatalytic activity as oxygen vacancies act as electron trap. Other than that, FESEM and HRTEM revealed that the ZnO nanorods originated from the centre, forming flower-like morphologies for ZnO, whereas the ZnO nanorods were distributed on rGO surface uniformly. This observation shows that rGO could prevent the aggregation of ZnO particles. In addition, the size of the ZnO nanorods in the nanocomposite was also smaller compared to the pure ZnO.

From adsorption in the dark experiment, ZnO/rGO nanocomposites show higher adsorptivity rate than ZnO. This adsorption rate also increased with increasing rGO loading in the nanocomposites. The adsorption property of the nanocomposites can be explained by the π - π stacking interaction between aromatic rGO and aromatic MB solution. From the photocatalytic experiment, ZnO/rGO nanocomposites also showed higher degradation rate than ZnO. This is due to the synergistic effects of smaller ZnO nanorod and the presence of rGO that acts as a photosensitizer during sunlight illumination. Among all samples, ZG1

showed the highest degradation rate and the stability of ZG1 was tested by repeating the photocatalytic experiment in six cycles. ZG1 were able to degrade almost clearly the MB solution, even after the sixth cycle, and the HRTEM image showed that the morphology was not significantly changed. Also from the photocurrent experiment, the results were in good agreement with the photocatalytic results. ZnO/rGO nanocomposites showed higher photocurrent response due to the photoexcited rGO under solar light irradiation. The use of rGO in the nanocomposite had an obvious effect on the overall application performance. This work confirmed that besides adsorption capability of rGO, it could also help in transporting of electrons contributing to the enhancement of the overall performance.

5.2 Future works

Besides photocatalytic application, it is reported that uniform one-dimensional ZnO nanorods have potential to be applied in solar cells, electronics, water-splitting, sensor devices, hydrogen production as well as life-science applications. So far, in the present investigation the ZnO, ZnO/rGO nanocomposite and rGO were successfully synthesized by microwave assisted route. ZnO nanorods are decorated onto the rGO sheets. In addition, the synthesized samples were characterized and have been applied in photocatalytic and photocurrent experiment and found that ZnO/rGO nanocomposite performed better than ZnO.

The method used for this work which is microwave method can be modified by varying the experimental parameters such as, stirring time, microwave power and microwave irradiation time to get other ZnO nanostructure, such as nanosheets, nanowire, nanoflakes, and etc. By obtaining various structure of ZnO, it is expected more applications can be done. Other materials such as titanium dioxide and iron oxide also can be added to the ZnO/rGO nanocomposite to form rGO-based hetero-nanostructure in order to enhance the performance of gas sensor devices. In the future, hopefully the results of this current work have a potential improve the large scale production.

REFERENCES

- Adams, V., Marley, J., & McCarroll, C. (2007). Prilocaine induced methaemoglobinaemia in a medically compromised patient. Was this an inevitable consequence of the dose administered? *British Dental Journal*, 203(10), 585–7.
- Adán-Más, A., & Wei, D. (2013). Photoelectrochemical properties of graphene and its derivatives. *Nanomaterials*, 3(3), 325–356.
- Ali, R., Azelee, W., Abu, W., & Teck, L. K. (2010). Zn/ZnO/TiO₂ and Al/Al₂O₃/TiO₂ Photocatalysts for the Degradation of Cypermethrin. *Modern Applied Science*, 59–67.
- Al-Rasheed, R. A. (2005). Water treatment by heterogeneous photocatalyst. Paper presented at 4th SWCC Acquired Experience Symposium, Jeddah, Saudi Arabia.
- Ambro, G., & Orel, Z. C. (2011). Microwave-assisted non-aqueous synthesis of ZnO nanoparticles. *Materials and Technology*, 45(3), 173–177.
- Ana, P. B. R. de F., Leandro, V. de F., Gisella, L. S., Fernando, A. S. M., Carla Cristina Almeida Loures, Salman, F., Túlio, L. dos S., & Silva, M. B. (2013). *Multivariate analysis in management, engineering and the sciences*. (L. Freitas, Ed.). InTech.
- Bai, S., Liu, X., Li, D., Chen, S., Luo, R., & Chen, A. (2011). Synthesis of ZnO nanorods and its application in NO₂ sensors. *Sensors and Actuators B: Chemical*, 153(1), 110–116.
- Chen, H., & Wang, L. (2014). Nanostructure sensitization of transition metal oxides for visible-light photocatalysis. *Beilstein journal of nanotechnology*, 5(2), 696–710.
- Choi, W., Lahiri, I., Seelaboyina, R., & Kang, Y. S. (2010). Synthesis of graphene and its applications: a review. *Critical Reviews in Solid State and Materials Sciences*, 35(1), 52–71.
- Colmenares, J. C., Luque, R., Campelo, J. M., Colmenares, F., Karpiński, Z., & Romero, A. A. (2009). Nanostructured photocatalysts and their applications in the photocatalytic transformation of lignocellulosic biomass. *Materials*, 2(4), 2228–2258.
- Durantini, J., Boix, P. P., Gervaldo, M., Morales, G. M., Otero, L., Bisquert, J., & Barea, E. M. (2012). Photocurrent enhancement in dye-sensitized photovoltaic devices with titania-graphene composite electrodes. *Journal of Electroanalytical Chemistry*, 683, 43–46.
- Stone, F. G. A. (1988). *Advances in organometallic chemistry*. Huelva, Spain: Elsevier.
- Fuente, J. de La. (2013). Reduced graphene oxide. *Graphenea*. Retrieved from <http://www.graphenea.com/pages/reduced-graphene-oxide#.Unnp8zeITK4>
- Ganguly, A., Sharma, S., Papakonstantinou, P., & Hamilton, J. (2011). Probing the thermal deoxygenation of graphene oxide using high-resolution in situ x-ray-based spectroscopies. *The Journal of Physical Chemistry C*, 115(34), 17009–17019.
- Gao, P. X., & Wang, Z. L. (2005). Nanoarchitectures of semiconducting and piezoelectric zinc oxide. *Journal of Applied Physics*, 97(4), 044304.

- Whittaker, G. (1997). A basic introduction to microwave chemistry. Retrieved from <http://homepages.ed.ac.uk/ah05/basicintro.html>.
- Gouws, S. (2012). Electrolysis. *InTech*. doi: 10.5772/48499
- Gusatti, M., do Rosário, J. D. A., de Campos, C. E. M., Kunhen, N. C., de Carvalho, E. U., Riella, H. G., & Bernardin, A. M. (2010). Production and characterization of ZnO nanocrystals obtained by solochemical processing at different temperatures. *Journal of Nanoscience and Nanotechnology*, 10(7), 4348–4351.
- Morkoç, H. & Özgür, Ü. (2009). General properties of ZnO. Zinc Oxide: Fundamentals, Materials and Device Technology. (pp. 1–75). Richmond, Virginia: Wiley.
- Hasan, K. (2012). *Graphene and ZnO nanostructures for nano-optoelectronic and biosensing applications* (Doctoral dissertation, Linköping University). Retrieved from <http://urn.kb.se/resolve?urn=urn:nbn:se:liu:diva-78697>
- Hickman, K. (2002). Nanomaterials: It's a Small, Small World. *ProQuest*. Retrieved from <http://www.csa.com/discoveryguides/nano/overview.php>
- Hofsäss, H., Kuo, C.-T., Chu, J. P., Feng, Z.-C., Hsieh, J.-H., Ginley, D., Huang, J., et al. (2013). A study of the electrical properties of graphene-incorporated direct-patternable ZnO thin films. *Thin Solid Films*, 529, 234–237.
- Hummers, W. S., & Offeman, R. E. (1957). Preparation of Graphitic Oxide. *Journal of the American Chemical Society*, 208(1937), 1937.
- Hedberg, J. (2013). Graphene sheets. Retrieved from <http://www.jameshedberg.com/scienceGraphics.php?sort=graphene&id=graphene-sheet-wavey>
- Janotti, A., Varley, J. B., Lyons, J. L., & Walle, C. G. Van De. (2012). Functional metal oxide nanostructures. (J. Wu, J. Cao, W.-Q. Han, A. Janotti, & H.-C. Kim, Eds.) Springer Series in Materials Science, 149. New York, NY: Springer.
- Jay, J. (2014). *Experiment on Cyclic Voltammetry*. Retrieved from <http://www.scribd.com/doc/215182326/Experiment-3>
- Johnston, H. (2010). Graphene pioneers bag nobel prize. *Institute of Physics*. Retrieved from <http://physicsworld.com/cws/article/news/2010/oct/05/graphene-pioneers-bag-nobel-prize>
- Kappe, C. O., Dallinger, D., & Murphree, S. S. (2009). Microwave synthesis – an introduction. *Practical Microwave Synthesis for Organic Chemistry: Strategies, Instruments, and Protocols* (pp. 1–10). Weinheim, Germany: Wiley.
- Kashyout, A. B., Soliman, H. M. A., Hassan, H. S., & Abousehly, A. M. (2010). Fabrication of ZnO and ZnO : Sb nanoparticles for gas sensor applications. *Journal of Nanomaterials*, 2010.
- Kasiri, M. B., & Khataee, a. R. (2011). Photooxidative decolorization of two organic dyes with different chemical structures by UV/H₂O₂ process: Experimental design. *Desalination*,

- Kauppila, J., & Viinikanoja, A. (2012). Electrochemical reduction of graphene oxide and its in situ spectroelectrochemical characterization. *Physical Chemistry Chemical Physics*. Retrieved from <http://www.utu.fi/en/units/sci/units/chemistry/research/mcca/Pages/Subpages of Functional Materials/Graphenes.aspx>
- Kim, Y.-K., & Min, D.-H. (2012). Simultaneous reduction and functionalization of graphene oxide by polyallylamine for nanocomposite formation. *Carbon Letters*, 13, 29 – 33.
- Lemma, T., & Yohannes, T. (2007). Poly(3-methylthiophene-co-3-octylthiophene) based solid-state photoelectrochemical device. *Journal of the Brazilian Chemical Society*. Retrieved from http://www.scielo.br/scielo.php?pid=S0103-50532007000400022&script=sci_arttext
- Li, B., & Cao, H. (2011). ZnO@graphene composite with enhanced performance for the removal of dye from water. *Journal of Materials Chemistry*, 21(10), 3346.
- Li, J. Y. (2008). Physical and electrical performance of vapor–solid grown ZnO straight nanowires. *Nanoscale Research Letters*, 4, 165 – 168.
- Li, Y., Gao, W., Ci, L., Wang, C., & Ajayan, P. M. (2010). Catalytic performance of Pt nanoparticles on reduced graphene oxide for methanol electro-oxidation. *Carbon*, 48(4), 1124–1130.
- Liang, Y., Wang, H., Sanchez Casalongue, H., Chen, Z., & Dai, H. (2010). TiO₂ nanocrystals grown on graphene as advanced photocatalytic hybrid materials. *Nano Research*, 3(10), 701–705.
- Lim, H. N., Nurzulaikha, R., Harrison, I., Lim, S. S., Tan, W. T., Yeo, M. C., Yarmo, M. a. & Huang, N. M. (2012). Preparation and characterization of tin oxide, SnO₂ nanoparticles decorated graphene. *Ceramics International*, 38(5), 4209–4216.
- Liu, F., Lu, L., Xiao, P., He, H., Qiao, L., & Zhang, Y. (2012). Effect of oxygen vacancies on photocatalytic efficiency of TiO₂ nanotubes aggregation. *Korean Chemical Society*, 33(7), 2255–2259.
- Liu, H., & Zhang, L. (2009). Microwave heating in organic synthesis and drug discovery. Shanghai, China: Intech.
- Mandal, S. S., & Bhattacharyya, A. J. (2012). Electrochemical sensing and photocatalysis using Ag – TiO₂ microwires. *Journal of Chemical Sciences*, 124(5), 969–978.
- Marcano, D. C., Kosynkin, D. V, Berlin, J. M., Sinitskii, A., Sun, Z., Slesarev, A., Alemany, L. B., Lu, W., & Tour, J. M. (2010). Improved synthesis of graphene oxide. *ACS nano*, 4(8), 4806–14.
- Nandita, D., & Amitava, D. (2004). *Semiconductor Devices: Modelling and Technology*. New Delhi, India: Prentice-Hall of India.

- Narayan, H., Alemu, H., Macheli, L., Sekota, M., Thakurdesai, M., & Rao, T. K. G. (2009). Role of particle size in visible light photocatalysis of congo red using $\text{TiO}_2\cdot[\text{ZnFe}_2\text{O}_4]_x$ nanocomposites. *Bulletin of Material Science*, 32(5), 499–506.
- National Aeronautics and Space Administration, Science Mission Directorate. (2010). *Microwaves*. Retrieved from Mission:Science website: http://missionscience.nasa.gov/ems/06_microwaves.html
- Olad, A. (1996). Polymer/Clay Nanocomposites. In B. Reddy (Ed.) *Advances in Diverse Industrial Applications of Nanocomposites*. (pp. 113 - 138). Tebriz, Iran: Intech
- Ong, W. L., Natarajan, S., Kloostra, B., & Ho, G. W. (2013). Metal nanoparticle-loaded hierarchically assembled ZnO nanoflakes for enhanced photocatalytic performance. *Nanoscale*, 5(12), 5568–75.
- Pakapongpan, S., Surareungchai, W., & Palangsantikul, R. (2011). Electrochemical study of methylene blue-carbon nanotubes nanohybrid modified glassy carbon electrode and its application for myoglobin detection. Paper presented at the *Pure and Applied Chemistry International Conference 2011*, Bangkok, Thailand.
- Park, S., & Ruoff, R. S. (2009). Chemical methods for the production of graphenes. *Nature Nanotechnology*. Retrieved from http://www.nature.com/nnano/journal/v4/n4/fig_tab/nnano.2009.58_F1.html
- Pillai, S. C., Periyat, P., George, R., McCormack, D. E., Michael, K., Hayden, H., Colreavy, J., et al. (2007). Synthesis of high temperature stable anatase TiO_2 photocatalyst. *The Journal of Physical Chemistry*, 4, 1605–1611.
- Prakash, A., Misra, S. K., & Bahadur, D. (2013). The role of reduced graphene oxide capping on defect induced ferromagnetism of ZnO nanorods. *Nanotechnology*, 24(9), 095705.
- R.G. Compton. (1989). *New techniques for the study of electrodes and their reactions*. (pp. 503). Oxford. UK: Elsevier.
- Sakthivel, S., Neppolian, B., Shankar, M. V, Arabindoo, B., Palanichamy, M., & Murugesan, V. (2003). Solar photocatalytic degradation of azo dye : comparison of photocatalytic efficiency of ZnO and TiO_2 . *Solar Energy Materials and Solar Cells*, 77(3), 65–82.
- Sakurai, K., & Mizusawa, M. (2010). X-ray diffraction imaging of anatase and rutile. *Analytical chemistry*, 82(9), 3519–22.
- Saleh, F. T. (2011). *Sensitization of semiconducting nano powder catalysts in photodegradation of medical drugs and microorganisms in water* Sensitization of semiconducting nano powder catalysts in photodegradation of medical drugs and microorganisms in water (Master's thesis, An-Najah National University, Nablus, Palestine). Retrieved from <http://scholar.najah.edu/content/sensitization-semiconducting-nano-powder-catalysts-photodegradation-medical-drugs-and>
- Singh, G., Choudhary, A., Haranath, D., Joshi, A. G., Singh, N., Singh, S., & Pasricha, R. (2012). ZnO decorated luminescent graphene as a potential gas sensor at room temperature. *Carbon*, 50(2), 385–394.

- Soltani, N., Saion, E., Hussein, M. Z., Erfani, M., Abedini, A., Bahmanrokh, G., Navasery, M., et al. (2012). Visible Light-Induced Degradation of Methylene Blue in the Presence of Photocatalytic ZnS and CdS Nanoparticles. *International journal of molecular sciences*, 13(10), 12242–58. Retrieved from <http://www.pubmedcentral.nih.gov/articlerender.fcgi?artid=3497270&tool=pmcentrez&rendertype=abstract>
- Srivastava, N. (2012). *Interface structure of graphene on SiC for various preparation conditions*. (Doctoral thesis, Carnegie Mellon University, Pittsburgh). Retrieved from <http://repository.cmu.edu/dissertations/90/>
- Stankovich, S., Dikin, D. A., Piner, R. D., Kohlhaas, K. A., Kleinhammes, A., Jia, Y., Wu, Y., et al. (2007). Synthesis of graphene-based nanosheets via chemical reduction of exfoliated graphite oxide. *Carbon*, 45(7), 1558–1565.
- Tan, L.-L., Ong, W.-J., Chai, S.-P., & Mohamed, A. R. (2013). Reduced graphene oxide-TiO₂ nanocomposite as a promising visible-light-active photocatalyst for the conversion of carbon dioxide. *Nanoscale Research Letters*, 8(1), 465. Retrieved from <http://www.pubmedcentral.nih.gov/articlerender.fcgi?artid=3827867&tool=pmcentrez&rendertype=abstract>
- Tang, L., Li, X., Ji, R., Teng, K. S., Tai, G., Ye, J., Wei, C., et al. (2012). Bottom-up synthesis of large-scale graphene oxide nanosheets. *Journal of Materials Chemistry*, 22(12), 5676.
- Tierney, J., & Westman, J. (2001). *Microwave assisted organic synthesis*. Retrieved from <https://www.erowid.org/archive/rhodium/pdf/microwave.organic.chemistry.review.pdf>
- Tschirch, J., Dillert, R., Bahnemann, D., Proft, B., Biedermann, A., & Goer, B. (2008). Photodegradation of methylene blue in water, a standard method to determine the activity of photocatalytic coatings? *Research on Chemical Intermediates*, 34(4), 381–392.
- Umar, M., & Aziz, H. A. (2013). *Photocatalytic Degradation of Organic Pollutants in Water* (pp. 195–208).
- Vijay Kumar, S., Huang, N. M., Yusoff, N., & Lim, H. N. (2013). High performance magnetically separable graphene/zinc oxide nanocomposite. *Materials Letters*, 93, 411–414.
- Wang, Z. L. (2004). Nanostructures of zinc oxide. (pp. 26–33). Atlanta. USA: Materials Today.
- Xu, S., Lao, C., Weintraub, B., & Wang, Z. L. (2008). Density-controlled growth of aligned ZnO nanowire arrays by seedless chemical approach on smooth surfaces. *Materials Research Society*. Retrieved from http://www.nanoscience.gatech.edu/paper/2008new/2008_dga.pdf
- Xu, T., Zhang, L., Cheng, H., & Zhu, Y. (2011). Significantly enhanced photocatalytic performance of ZnO via graphene hybridization and the mechanism study. *Applied Catalysis B: Environmental*, 101(3-4), 382–387.
- Yang, Y., & Liu, T. (2011). Fabrication and characterization of graphene oxide/zinc oxide nanorods hybrid. *Applied Surface Science*, 257(21), 8950–8954.

- Yao, W.-T., Yu, S.-H., Liu, S.-J., Chen, J.-P., Liu, X.-M., & Li, F.-Q. (2006). Architectural control syntheses of CdS and CdSe nanoflowers, branched nanowires, and nanotrees via a solvothermal approach in a mixed solution and their photocatalytic property. *The Journal of Physical Chemistry. B*, 110(24), 11704–10.
- Yasuhiro Hatsugai. (2010). Scattering of Dirac Fermions with Doubling. Retrieved from http://jpsj.ipap.jp/news/jpsj-nc_74.html
- Ye, F., Peng, Y., Chen, G.-Y., Deng, B., & Xu, A.-W. (2009). Facile Solution Synthesis and Characterization of ZnO Mesocrystals and Ultralong Nanowires from Layered Basic Zinc Salt Precursor. *The Journal of Physical Chemistry C*, 113(24), 10407–10415.
- Yeh, T.-F., Cihlář, J., Chang, C.-Y., Cheng, C., & Teng, H. (2013). Roles of graphene oxide in photocatalytic water splitting. *Materials Today*, 16(3), 78–84.
- Yi, S.-H., Choi, S., Jang, J.-M., Kim, J.-A., & Jung, W.-G. (2008). Patterned Growth of a Vertically Aligned Zinc Oxide Rod Array on a Gallium Nitride Epitaxial Layer by Using a Hydrothermal Process. *Journal of the Korean Physical Society*, 53(1), 227–231.